4 Metal oxide nanoparticles

Metal oxides are a broad class of materials, both naturally-occurring and synthetic, exhibiting diverse properties and applications. Metal oxide nanoparticles (NPs) have likewise attracted significant interest. This chapter discusses widely-studied oxide NP systems such as *iron oxide NPs*, *silicon oxide NPs*, *titanium oxide NPs*, *zinc oxide NPs*, and *rare earth oxide NPs*.

4.1 Iron oxide nanoparticles

Iron oxide (Fe_3O_4 familiarly known as *magnetite*, and its oxidized species *maghemite* Fe_2O_3) forms highly *magnetic* nanoparticles, as iron is one of the most ferromagnetic elements in the periodic table. The sizable magnetic moment of iron oxide NPs (IONPs) – i.e. *superparamagnetism* – is directly related to the nanoscale dimensions of the particles, specifically the *single crystalline* domains they comprise of. In a somewhat simplistic picture, the electron spins in such single-domain IONPs are all oriented in the same direction, producing a strong local magnetic field (Fig. 4.1). IONPs are thus commonly referred to as "magnetic NPs" or MNPs. Furthermore, below a certain size threshold (typically around 20 nm for IONPs), the magnetic properties of the NPs become *size-dependent* due to the enhanced contribution of magnetic and energy properties of the nanoparticle *surface* as compared to the *core* (or "bulk" component).

While a detailed discussion of the fundamental physical properties of IONPs, particularly the size-dependent magnetic properties, is beyond the scope of this book, it is safe to say that the pronounced *magnetism* of IONPs (and other magnetic NPs for

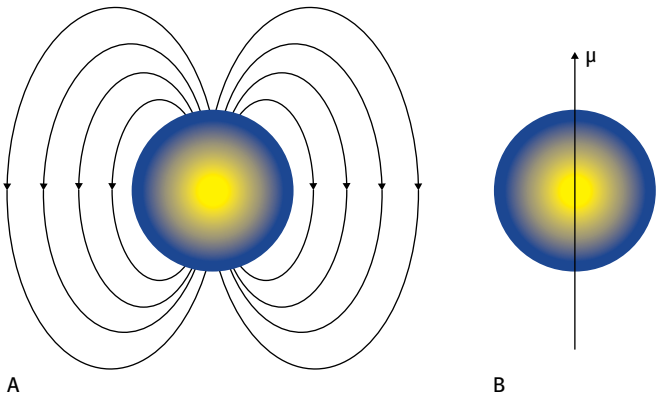

Fig. 4.1: Iron oxide nanoparticles. **A:** The magnetic field around the nanoparticle. **B:** Direction of magnetic moment.

that matter) is the defining scientific and technological feature of these NP species. Indeed, the interactions of IONPs with magnetic fields are the primary attraction of these systems for biological imaging and therapeutics, and representative examples of this vast research area are presented below.

IONPs are amenable to biological applications since iron is an integral participant in many physiological processes. Primary among these is iron's role in oxygen and carbon dioxide transport in the bloodstream (as part of the *hemoglobin* in red blood cells). Accordingly, IONPs are presumed to exhibit minimal toxicity, and could be recycled and/or discarded via natural biodegradation pathways in the human body. Indeed, intensive R&D efforts in this field have already resulted in the commercialization of several pharmaceutical formulations containing IONPs.

Many iron oxide NP *synthesis schemes* have been developed. Synthetic routes for production of magnetic NPs are not complex, however they vary significantly in terms of particle homogeneity, stability of the NP products, and their biocompatibility. Solution-based synthesis has been widely used to generate IONPs. Most methods start with iron salts or iron complexes, which are subsequently converted to IONPs on reaction with oxygen donors at elevated temperatures. Solution-based syntheses can be divided into *aqueous phase* and *organic phase* processes. *Water-based* synthetic methods are easy to implement and usually produce large quantities of biocompatible particles. The downside of such techniques is low particle uniformity, i.e. less monodispersity. *Organic phase* magnetic NP synthesis generally yields more homogeneous reaction products, albeit particle coating with molecules displaying hydrophilic moieties is then required for further use in biological applications (or for other applications carried out in aqueous environments).

Figure 4.2A illustrates a widely used method for synthesizing crystalline and monodisperse γ-Fe_2O_3 NPs (e.g. the *maghemite* sub-family of iron oxides). Iron pentacarbonyl, $Fe(CO)_5$, is treated with oleic acid at 100°C, forming an iron-oleic acid metal complex. Upon heating at a higher temperature of 300°C, the iron-oleic acid complex decomposes to form Fe nanoparticles which can be converted to γ-Fe_2O_3 nanoparticles via controlled oxidation with a mild oxidant, trimethylamine oxide, $(CH_3)_3NO$. Figure 4.2B depicts an alternative method, in which co-precipitation of

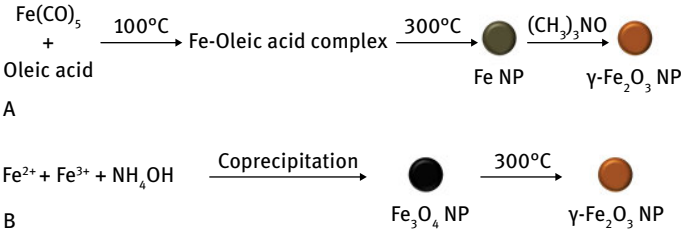

Fig. 4.2: Common synthetic processes for production of iron oxide nanoparticles.

Fe^{2+} and Fe^{3+} ions in the presence of ammonium hydroxide (NH_4OH) in aqueous medium results in the formation of *magnetite* (Fe_3O_4) nanoparticles, which can be converted to Fe_2O_3 NPs through oxidation in air at 300°C.

Developments of IONP synthesis methods have led to intriguing discoveries, such as the creation of *hollow* IONPs. A. P. Alivisatos and colleagues at the Lawrence Berkeley Laboratory, for example, found that oxidation of metallic iron NPs at between 200°C–300°C led to formation of hollow and core-shell IONPs (Fig. 4.3). This interesting phenomenon was ascribed to rapid diffusion of the oxidized iron ions from the metallic core outwards to the iron oxide shell of the NP, leaving behind "vacancies" which eventually coalesced into larger empty spaces inside the nanoparticles.

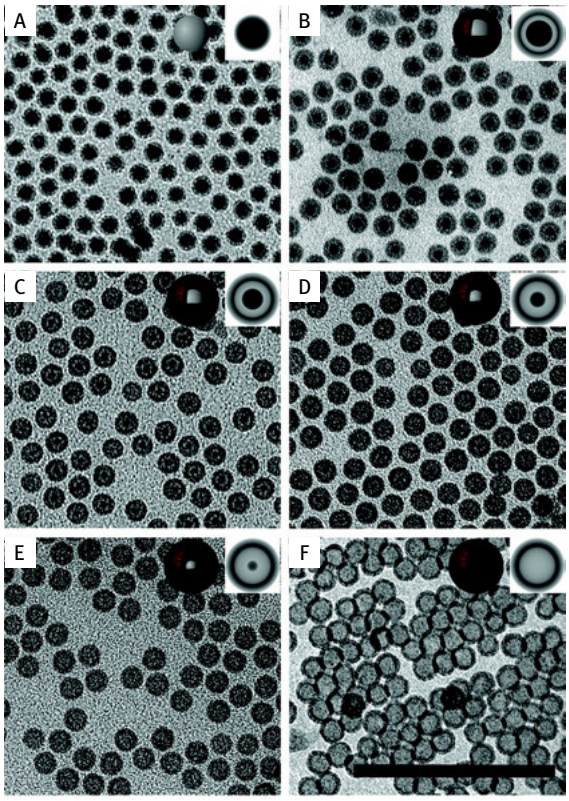

Fig. 4.3: Hollow iron oxide nanoparticles. Electron microscopy images of iron nanoparticles exposed to oxygen gas for increasing lengths of time. Nanoparticles with different configurations of iron oxide shell/iron core/voids are formed. Schematic depictions of nanoparticle structures and cross-section projections are shown in the top right of each image. Scale bar corresponds to 100 nm. Reprinted with permission from Cabot et al., *JACS* **129** (2007), 10358–10360, © 2007 American Chemical Society.

As with the other types of NPs discussed in this book, chemical functionalization of IONPs is a key feature of their wide applicability, particularly in biology and biomedicine. Numerous synthetic routes have been introduced for covalent display of chemical and biological recognition elements, enzymes, peptides, oligonucleotides, and other molecular constituents on IONP surfaces. *Noncovalent* association of hydrophobic/hydrophilic layers on IONPs has also been widely carried out. Such shells

generally prevent NP aggregation, but also play critical roles in many instances, including NP biocompatibility, minimizing immune response, and enabling NP passage through physiological barriers such as the blood-brain barrier (BBB) and cell membranes. Furthermore, the molecular layers encapsulating the iron oxide core can act as "protective shields", preventing enzymatic degradation in the bloodstream and extracellular space.

Figure 4.4 depicts a strategy for construction of functionalized IONPs with molecular recognition properties via a combined noncovalent/covalent approach. The single-step synthetic procedure, developed by W. Tan and colleagues at the University of Florida, enclosed IONPs within a hydrophobic layer comprising of phospholipid residues covalently attached to *hydrophilic* recognition elements. The approach is generic, as different residues can be attached to the phospholipids. Specifically, the researchers demonstrated the concept by conjugating *oligonucleotides* (DNA fragments) to the phospholipids. Binding the functionalized IONPs was achieved through *hybridization* between the NP-displayed DNA and its complementary oligonucleotide target. Alternatively, *specific protein binding* could be accomplished through the use of *aptamers* – short DNA fragments designed to recognize and bind protein targets. Modified IONPs such as those shown in Figure 4.4 can be functionalized with multiple, different ligands, and the hydrophilic residues extending from the NP surface had a further role in stabilizing the particles in aqueous solutions.

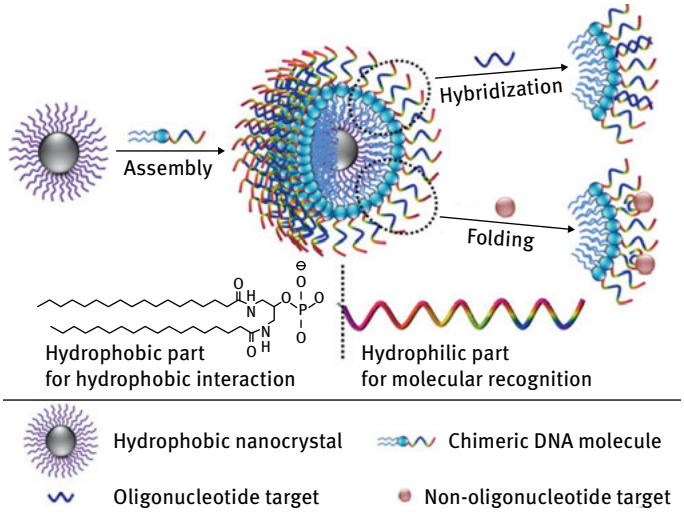

Fig. 4.4: Iron oxide nanoparticles displaying biomolecular recognition elements. The nanoparticles are coated with a layer of phospholipid molecules functionalized with hydrophilic residues (DNA sequences). Target recognition is achieved either through DNA hybridization (top route) or peptide-binding and consequent folding (bottom route). Reprinted with permission from Chen et al., *JACS* **134** (2012), 13164–13167, © 2012 American Chemical Society.

Another example of IONP functionalization through noncovalent interactions is presented in Figure 4.5. In this simple yet powerful system, developed by D. G. Anderson and colleagues at MIT, the IONPs were interspersed with *cationic lipids* which prevented aggregation of the NPs in water solutions. The NPs were subsequently loaded with oligonucleotides (either DNA, or "small-interfering RNA", siRNA; widely employed as a tool for "gene silencing" as it interferes with gene expression pathways) which were bound to the cationic residues through electrostatic attraction. The assemblies generated were quite uniform in size, resilient in physiological solutions, and could efficiently deliver their oligonucleotide cargoes to cell targets.

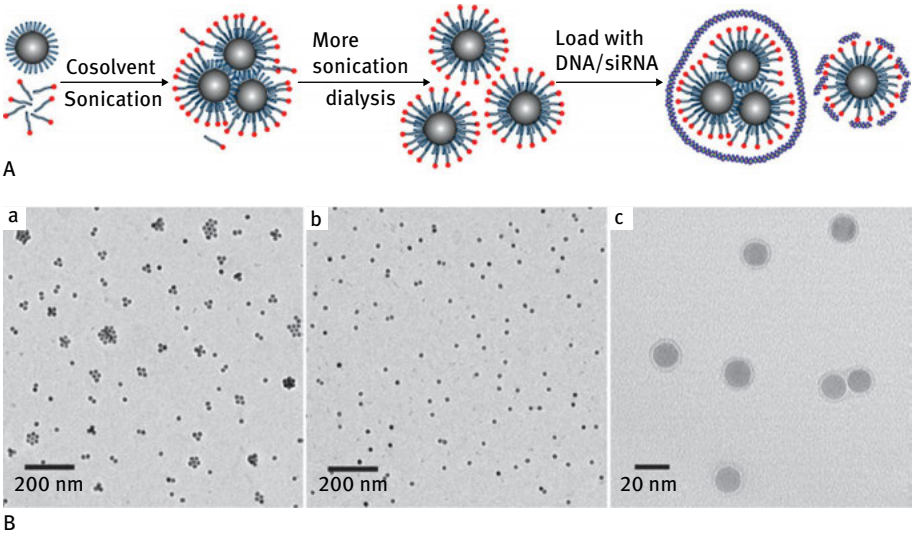

Fig. 4.5: DNA delivery through lipid coating of iron oxide nanoparticles. **A:** Experimental scheme: the iron oxide nanoparticles are interspersed and coated with cationic lipids. Following dispersion through sonication and dialysis the lipid-coated nanoparticles are mixed with DNA or RNA which associate with the nanoparticles through electrostatic attraction. **B–D:** Electron microscopy images showing different stages in the process: **B** cationic lipid/iron oxide nanoparticle aggregates; **C** dispersed lipid-coated iron oxide nanoparticles; **D** DNA-associated lipid-coated iron oxide nanoparticles. Reprinted with permission from Jiang et al., *Nano Lett.* **13** (2013), 1059–1064, © 2013 American Chemical Society.

One of the major advantages of using IONPs such as those shown in Figures 4.4 and 4.5 for biomolecular targeting is the possibility of using an externally-applied *magnetic field* for physical separation and spatial manipulation of the NPs. Magnetically-guided targeting has been successfully demonstrated, for example, for the DNA/RNA-loaded IONPs prepared according to the scheme in Figure 4.5. In the experiment (summarized in Fig. 4.6) the researchers loaded the IONPs with DNA encoding for green fluorescent protein (GFP), a fluorescence-emitting protein. As shown in Figure 4.6, placing the

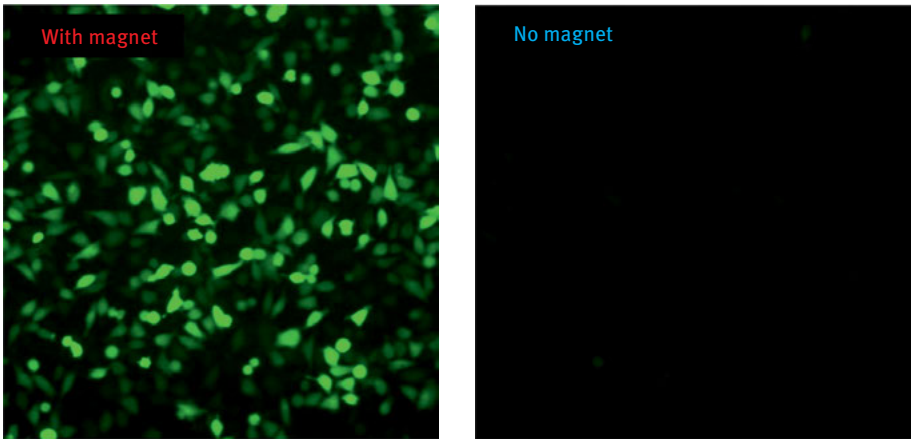

Fig. 4.6: Magnetic targeting of bio-functionalized iron oxide nanoparticles. Fluorescence microscopy images showing the effect of placing suspensions of cells and DNA/lipid-coated iron oxide nanoparticles in a magnetic field. The DNA is encoded for the green fluorescent protein (GFP), resulting in enhanced fluorescence of the cells incubated with the nanoparticles in the presence of a magnet (top image). Reprinted with permission from Jiang et al., *Nano Lett.* **13** (2013), 1059–1064, © 2013 American Chemical Society.

cells in a magnetic field gave rise to pronounced fluorescence (due to GFP expression by the DNA-transfected cells). This effect was ascribed to magnetically-induced increased concentration of the IONPs on the cell surface, consequently enhancing DNA delivery into the cell.

One of the early applications of IONPs was as *contrast agents* in magnetic resonance imaging (MRI). MRI is a powerful, noninvasive imaging technology based on the magnetic resonance signals of water protons' nuclei. The magnetic signals are highly sensitive to their chemical/biological environments, thereby providing detailed spatial information on organs and tissues. The significant role of IONPs in MRI stems from the shifts and in particular the attenuation of magnetic resonance signals of atoms in the vicinity of ferromagnetic atoms such as iron. Accordingly, accumulation of IONPs in cells and tissues generally results in substantially lower image brightness – e.g. higher contrasts with surrounding tissue areas not containing IONPs.

Numerous examples of IONP use in bio-imaging have been reported. Figure 4.7 depicts an MRI experiment utilizing IONPs coated with oleic acid (to prevent aggregation), which were further encapsulated within *oil micro-emulsions* (essentially microscale oil drops). When these NP assemblies were incubated with human cells the IONPs were taken up by the cells, thus allowing visualization of these cell populations thanks to enhanced contrast in the MRI images (Fig. 4.7B). While the oil-based formulations clearly promoted cell entry of IONPs, G. A. F. van Tilborg and colleagues at the University of Utrecht, Netherlands, found that the oil emulsions had an overall toxic effect, thereby limiting the practical impact of the strategy. Nevertheless, the

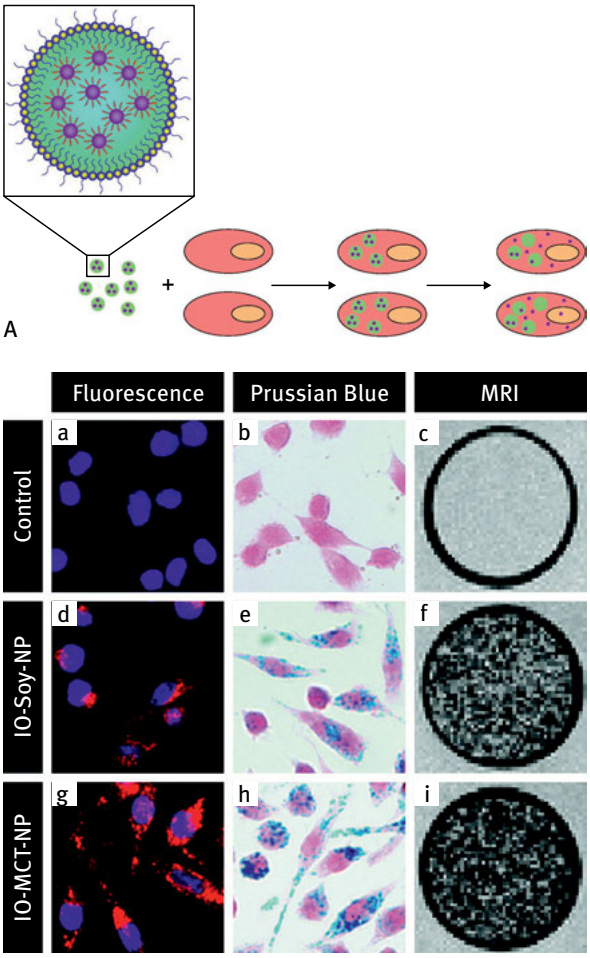

Fig. 4.7: Oil-encapsulated iron oxide nanoparticles for magnetic resonance imaging (MRI). **A:** Experimental scheme: the iron oxide nanoparticles are encapsulated within oil drops (i.e. micro-emulsions); following incubation with cells, the oil drops containing the iron oxide nanoparticles insert into the cells and subsequently release the nanoparticles in the cell interior. **B:** Results obtained for different formulations. **a–c:** control (no iron oxide nanoparticles; **d–f:** iron oxide nanoparticles embedded within soy oil micro-emulsion; **g–i:** iron oxide nanoparticles embedded within medium chain triglyceride oil (MCT) micro-emulsion. The fluorescence microscopy images (left column) depict the nuclei in blue, while the red fluorescent areas correspond to fluorescently-labeled nanoparticles taken up by the cells; Prussian blue (middle column) stains the iron nanoparticles within the cells; the MRI images (right column) show cell populations in which the iron oxide nanoparticles attenuated the magnetic resonance signals (i.e. darker areas). Reprinted with permission from van Tilborg et al., *Bioconjugate Chem.* **23** (2012), 941–950, © 2012 American Chemical Society.

experiments summarized in Figure 4.7 underscore the fact that IONPs can be transported into cells through diverse chemical avenues and successfully employed in MRI applications.

Localized heating of the NP environment through application of alternating magnetic fields (also referred to as *magnetic hyperthermia*) is one of the most important and therapeutically-promising phenomena associated with IONPs. This well-known effect stems from heat dissipation when the direction of the iron's electron spins is continuously inverted by an alternating magnetic field, and it provides a powerful therapeutic tool. For example, IONPs can be targeted to tumors by chemical means (surface-display of tumor recognition elements) or physical strategies (i.e. an external magnet directing the nanoparticle to the tumor area). An alternating magnetic field can then be applied to destroy the tumor via localized magnetic hyperthermia (Fig. 4.8).

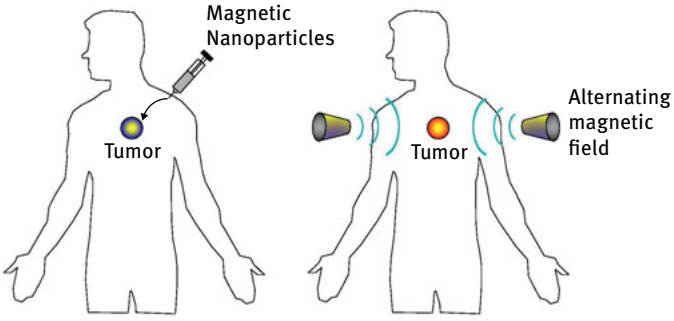

Fig. 4.8: Anti-tumor therapy using magnetic hyperthermia. Iron oxide nanoparticles are injected into the body and accumulate in a tumor area by chemical or physical means. An externally-applied alternating magnetic field subsequently induces localized heating of the nanoparticles at the tumor site through magnetic hyperthermia, destroying the tumor.

As expected, IONP-assisted cancer therapy has attracted intense interest in recent years. Several central issues in this field are illustrated in Figure 4.9. A major impediment of IONP delivery to their site of action, outlined by P. Couvreur and colleagues at Universite Paris-Sud, France, concerns inhibited transport within blood vessels (Fig. 4.9A). Upon injection into the bloodstream, IONPs, like other foreign objects, are quickly coated with a layer of *opsonins* – a class of blood-plasma proteins. Opsonin coating triggers a prominent physiological clearance mechanism, relying on capture by opsonin-binding antibodies present on the surface of macrophage cells ("Kupffer cells") within epithelial tissues (Fig. 4.9A). To avoid this clearance route and extend blood circulation times, IONPs can be coated with *polyethylene glycol (PEG)*, a commonly used biologically-inert polymer endowing "stealth" properties to the IONPs (Fig. 4.9B). Subsequent accumulation of IONPs in tumors can then be achieved ei-

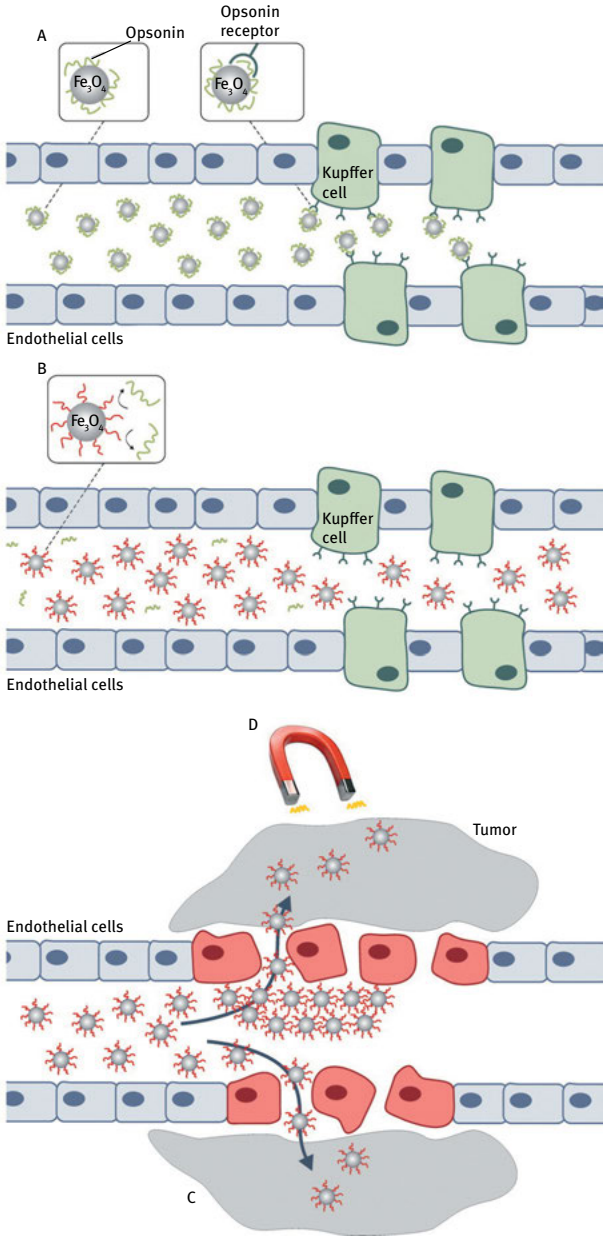

Fig. 4.9: Iron oxide nanoparticles in cancer therapy. **A:** The nanoparticles are coated with opsonins and consequently captured by anti-opsonin antibodies on epithelial cells. This process inhibits nanoparticle transport in blood vessels. **B:** Coating the nanoparticles with polyethylene glycol makes them biologically-inert. **C:** The nanoparticles can reach the tumor due to the high leakage of blood vessels around tumors; **D:** the iron oxide nanoparticles can be targeted via application of an external magnetic field. Reprinted with permission from van Reddy et al., *Chem. Rev.* **112** (2012), 5818–5878, © 2012 American Chemical Society.

ther through the intrinsic permeability and leakage of blood vessels around tumors (Fig. 4.9C), or by physical targeting via an externally-applied magnetic field (Fig. 4.9D).

Other biological applications of magnetic hyperthermia have been proposed. Figure 4.10 portrays an experiment in which localized heating induced by IONPs in an alternating magnetic field was employed as a vehicle for "remote controlled" enzyme activation. The experimental setup, designed by S. Daunert and colleagues at the University of Miami, comprised of enzyme molecules and IONPs embedded within a rigid hydrogel (transparent water-containing silica network). The enzyme selected by the researchers (dehalogenase) is *thermophilic*, i.e. it functions optimally at elevated temperatures (around 70 °C). Indeed, as shown in Figure 4.10, no enzymatic activity was observed at room temperature; however, on placing the sample in an alternating magnetic field enzyme activity was triggered by the increased temperature generated locally within the hydrogel by the encapsulated IONPs.

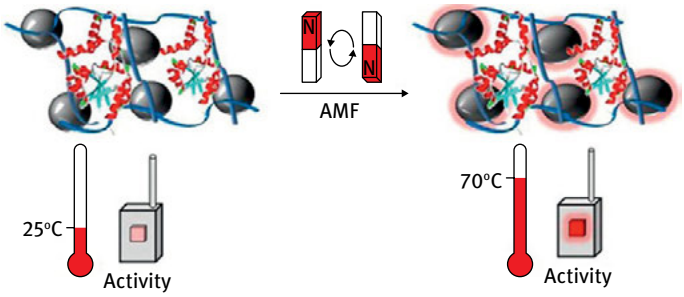

Fig. 4.10: "Remote control" enzyme catalysis via magnetic hyperthermia of iron oxide nanoparticles. Experimental scheme: the enzyme molecules (dehalogenase) and iron oxide nanoparticles are incorporated within a hydrogel matrix. At room temperature no activity of the thermophilic enzyme is observed. Upon application of an alternating magnetic field, localized heating is induced by the iron oxide nanoparticles (hyperthermia effect), increasing the temperature within the gel and activating the enzyme. Reprinted with permission from Knecht et al., *ACS Nano* **6** (2012), 9079–9086, © 2012 American Chemical Society.

The use of external magnetic fields for both spatial manipulation of IONPs as well as for induction of physical processes such as localized heating have opened up dramatic possibilities for IONPs in the emerging field of "theranostics" – combining both *therapeutics* and *diagnostics* in the same delivery vehicle. Figure 4.11 outlines typical modulations of IONPs for theranostic applications. The magnetic iron oxide core serves as the vehicle for spatial manipulations (via application of an external magnetic field), conduit for magnetic hyperthermia, and contrast agent in MR imaging. The molecular coating surrounding the magnetic core exhibits complementary functionalities, including delivery of therapeutic cargoes, display of recognition elements for cell- and tissue-targeting, and providing NP biocompatibility.

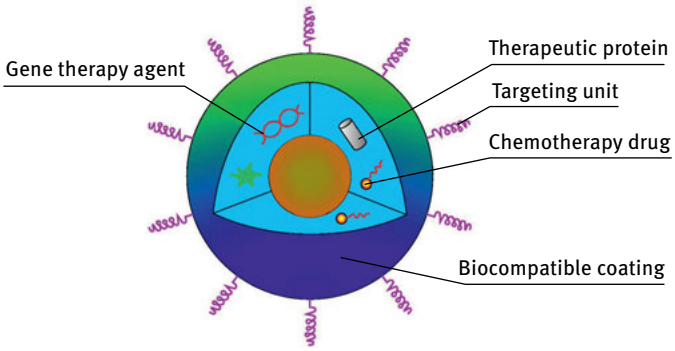

Fig. 4.11: Bio-functionalized iron oxide nanoparticles for theranostic applications. The generic scheme highlights different functional constituents of iron oxide nanoparticle assemblies exhibiting therapeutic and diagnostic applications.

Figure 4.12 presents an example of functionalized IONPs used for theranostics. The IONP system, designed by X. Chen and colleagues at the National Institutes of Health, US, enabled both delivery of a cancer therapeutic agent as well as imaging of the tumor area by MRI. Specifically, the IONPs were first treated with *dopamine*, rendering them hydrophilic (Fig. 4.12A). The NPs were then coated with *human serum albumin (HSA)* – an abundant human protein functioning here both as a vehicle for attaining biocom-

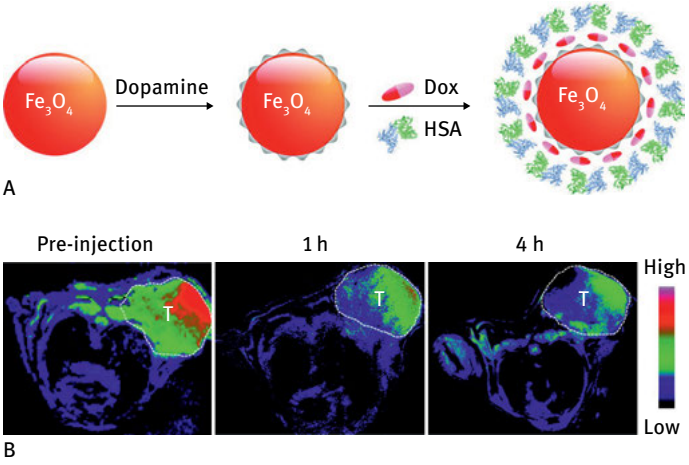

Fig. 4.12: Cancer theranostics with iron oxide nanoparticles. **A:** System design: iron oxide nanoparticles first coated with hydrophilic moieties (dopamine) and subsequently with a biocompatible human serum albumin layer and doxorubicin (Dox), an antitumor agent. **B:** Magnetic resonance images showing accumulation of the iron oxide nanoparticles in the tumor area, effectively quenching (darkening) of the MRI signals. Reprinted with permission from Quan et al., *Mol. Pharm.* **8** (2011), 1669–1676, © 2011 American Chemical Society.

patibility, and further as conduit for delivery of *doxorubicin (Dox)*, a known antitumor drug agent. This composite system was shown to target cancerous tissues, enabling their visualization by attenuating the magnetic signal in the MR image (Fig. 4.12B). Furthermore, the experimental data indicated that Dox was gradually released from the NP assemblies, leading to sustained blockage of tumor growth.

While IONPs hold great promise as a biomedical platform and, as mentioned above, are believed to be more physiologically benign compared to other inorganic NP families, there are inherent risks in their expanding uses, specifically with regard to longer-term biological/toxic effects. Studies have indeed pointed to potential hazards associated with IONPs. The formidable oxidizing capacity of iron oxide might lead to the generation of *reactive oxygen species (ROS)* – a major toxic factor implicated in various diseases and pathological conditions. The molecular layers and residues displayed on IONP surfaces are another potential source of adverse biological effects, in particular due to interference with cellular processes and signaling pathways. Several IONP species have been found, for example, to trigger inflammation pathways and induce liver damage in animal studies. It should be noted, however, that the physiological effects of IONPs are strongly dependent on their properties – size, composition, morphology, and biological functionalization. Overall, as in other novel and innovative NP-based therapeutics, research is still needed to systematically characterize the parameters affecting stability, degradation, long-term bio-distribution, and toxicity of IONPs. This knowledge would be essential to assess the future contributions of these fascinating NPs to biomedicine and therapeutics.

4.2 Titanium oxide nanoparticles

Titanium oxide (TiO_2 or *titania*) has long been utilized in industrial applications as a pigment, stabilizer in semi-solid materials such as toothpastes, and as a photocatalyst – for example catalyzing water splitting under ultraviolet (UV) light irradiation. The advent of nanotechnology in recent years has led to the creation of new TiO_2 nanostructures exhibiting intriguing properties. At the same time, a wealth of new applications based on TiO_2 nanoparticles has been reported. The prominent role of TiO_2 NPs in the rapidly growing solar energy field, in particular, has led to considerable research. While nanostructured TiO_2 can be found in various devices and technologies, this section focuses on TiO_2 NPs, their properties, and uses.

Numerous procedures for TiO_2 NP synthesis have been reported. These include chemical vapor deposition (CVD), popular with other types of semiconductor NPs, and direct oxidation of metallic titanium. Most *solution-based* synthesis schemes rely on hydrolysis of titanium ion (Ti^{4+}) precursors, usually of the type $Ti(OR)_4$, in which R corresponds to an alkyl moiety. The precursor molecules are dissolved in aqueous solutions, leading to formation of titanium hydroxide, $Ti(OH)_4$, complexes which are subsequently hydrothermally transformed (usually at high temperatures, >100°C) to

titanium oxide. Similar to other NP systems, *surfactant-mediated* synthesis protocols have been introduced, making possible preparation of TiO_2 NPs coated with surfactant layers which prevent aggregation and enable dissolution in different solvents. Attaining NP uniformity is considered a major challenge in TiO_2 NP synthesis, although in some applications the size distribution and NP morphologies do not have a significant impact on the material properties. Indeed, significant progress has been made in recent years towards development of synthetic procedures for the production of monodisperse TiO_2 NPs. A common strategy produces size-tunable TiO_2 NPs by varying the concentration of the *capping agent* (usually the surfactant molecules) as well as the solvent medium in which the reaction takes place.

TiO_2 is an indirect and wide bandgap semiconductor and thus, in principle, the efficiencies of light absorption and transfer of electrons from the valence band to the conduction band are limited. However, similar to semiconductor quantum dots, the energy bandgaps in TiO_2 NPs are shifted compared to the bulk material, enabling optical tuning via modulation of the NP dimensions. Indeed, light absorption can be enhanced as the size of the TiO_2 NPs is reduced, opening up new avenues for electro-optical and photonic applications. Since bare TiO_2, which is a wide bandgap semiconductor, absorbs energy in the ultraviolet (UV) region of the electromagnetic spectrum, the applicability of the pure material is limited in optical and photovoltaic devices. Various approaches have been implemented to overcome this limitation; primary among these is doping of TiO_2 with other molecular species, referred to as sensitizers, which exhibit lower energy bandgaps. The sensitizers absorb light in the visible (or infrared) regions and the excited electrons can then be further transferred into the conduction band of TiO_2 (Fig. 4.13). Maximizing the efficiency of charge transfer from the sensitizer to the TiO_2 NPs is a crucial factor in such coupled sensitizer/TiO_2 systems. Among the parameters contributing to effective transfer are the overlap between energy levels of the TiO_2 and sensitizer and properties of the interface between the two substances.

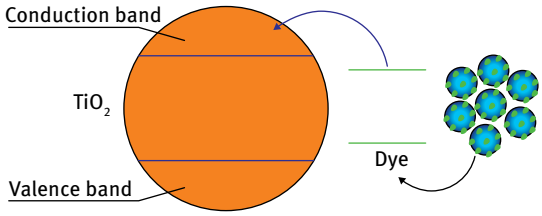

Fig. 4.13: The effect of sensitizers associated with TiO_2 nanoparticles. Excited electrons are transferred from the sensitizer dye exhibiting lower bandgap onto the conduction band of TiO_2.

Organic dyes act as sensitizers in *dye-sensitized solar cells (DSSCs)* – an active research area in which TiO_2 NPs constitute a core electron transport component. The basic DSSC configuration is shown in Figure 4.14. Light is absorbed by organic dyes (usually transition metal complexes) attached to the TiO_2 NPs. The photo-excited electrons are

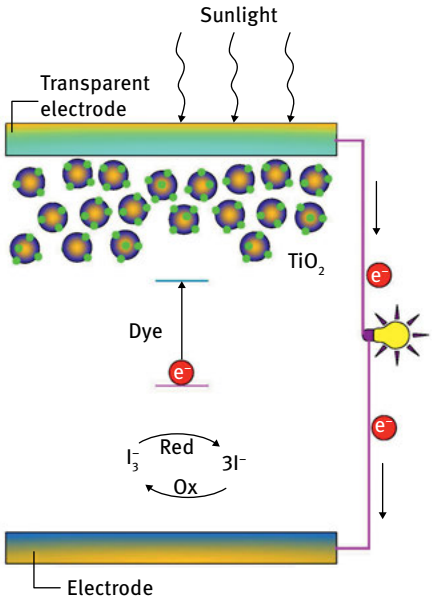

Fig. 4.14: Diagram showing the operation of a dye-sensitized solar cell (DSSC) utilizing TiO_2 nanoparticles. Electrons are excited in the dye molecules (shown as green spots attached to the TiO_2 nanoparticles). From the dye the electrons are transferred to the TiO_2 conduction band and onto the electrode. The electrons are regenerated through the redox reaction of the electrolyte (the I_3^-/I^- pair).

rapidly transferred to the conducting band of the TiO_2 and transported to one of the electrodes. At the same time, reduced/oxidized (redox) pairs (usually I^-/I_3^-, denoted as the *electrolytes*) embedded in the cell are responsible for providing the electrons to reduce the sensitizer to its initial state, simultaneously receiving the electrons from the back electrode and thereby closing the electrical circuit.

While the types of dyes and electrolytes (acting as redox couples) have been shown to play central roles in affecting the efficiency of DSSCs, the TiO_2 NPs also significantly shape solar cell performance. The *interface* between the TiO_2 NPs and the dyes, in particular, is critical, as it determines the extent of electron-transfer from the dye to the conduction band on the one hand, and the occurrence of electron-hole recombination processes which adversely influence cell efficiency on the other. Accordingly, various "interface engineering" strategies designed to reduce or inhibit electron-hole recombination have been reported. Deposition of semi-insulating layers on the TiO_2 NPs, for example, has been a common strategy – allowing charge transfer into the conduction band while at the same time preventing electron-hole recombination.

Numerous DSSC designs have been introduced containing diverse TiO_2 NP layer configurations and morphologies. Most solar cell constructs, in fact, utilize nanostructured or meso-structured TiO_2 films rather than TiO_2 nanoparticles per se. There have been reports, however, of using actual TiO_2 NPs. Figure 4.15 depicts a cell design in which an ordered array of hollow TiO_2 nanotubes was directly synthesized on a transparent electrode and integrated within a conventional DSSC setup. The TiO_2 nanotubes, synthesized by C. A. Grimes and colleagues at Penn State Univer-

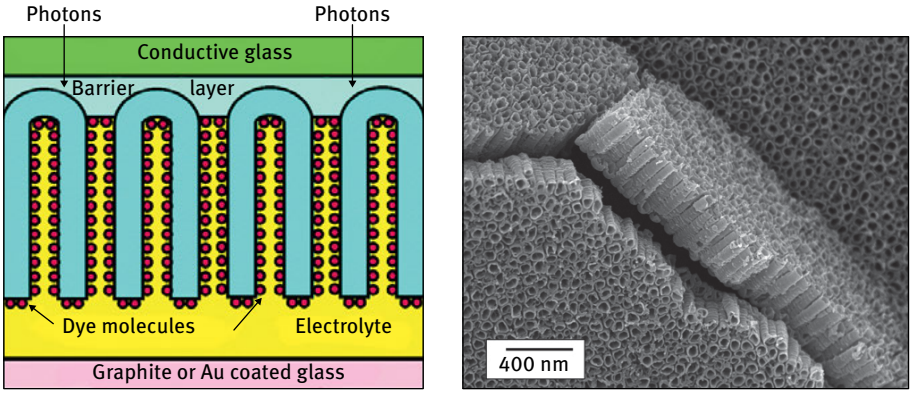

Fig. 4.15: Dye-sensitized solar cell using TiO_2 nanotubes. **A:** Diagram of the cell. The TiO_2 nanotubes (blue) are embedded within the electrolyte layer (yellow) and the organic dye molecules (sensitizer species, brown circles) are adsorbed onto the nanotube surface. **B:** Electron microscopy image of the TiO_2 nanotube array. Reprinted with permission from Mor et al., *Nano Lett.* **6** (2006), 215–218, © 2006 American Chemical Society.

sity through oxidation of a thin titanium film deposited on the electrode surface, were further doped with photon-absorbing metal-organic dyes and exhibited excellent electron transport properties as well as optical transparency – the two critical parameters which affect performance of the solar cell.

As indicated above, the use of bare TiO_2 nanostructures (i.e. those without doping or addition of sensitizer dye molecules) in solar cells is limited because of the large bandgap (in the ultraviolet spectral region), meaning potential absorption of only a small percentage of sunlight. However, the recent discovery of "black" TiO_2 NPs promises to dramatically expand the use of TiO_2 NPs in solar cells (and other applications). Black TiO_2 NPs ("black" refers to the sample appearance, which stands in contrast to white unmodified TiO_2 NPs) have been produced by hydrogen treatment of crystalline TiO_2 NPs. Remarkably, it has been found that the single-step crystallization/hydrogenation process yields NPs with much smaller bandgaps, effectively shifted to the visible region. While the exact mechanistic aspects underlying the unique photophysical properties of black TiO_2 have not been fully elucidated, the altered bandgap properties are believed to arise from formation of a "core-shell" structure in which the crystalline TiO_2 core of the nanoparticle is surrounded by partly reduced hydrogenated TiO_2 layer. Figure 4.16 shows black TiO_2 NPs synthesized by F. Huang and colleagues at the Chinese Academy of Sciences by treatment of conventional TiO_2 NPs with hydrogen plasma. Indeed, as shown in the microscopy image in Figure 4.16A, a thin amorphous layer appears to encase the crystalline TiO_2 core. The hydrogenated TiO_2 NPs were indeed found to exhibit dramatically-enhanced

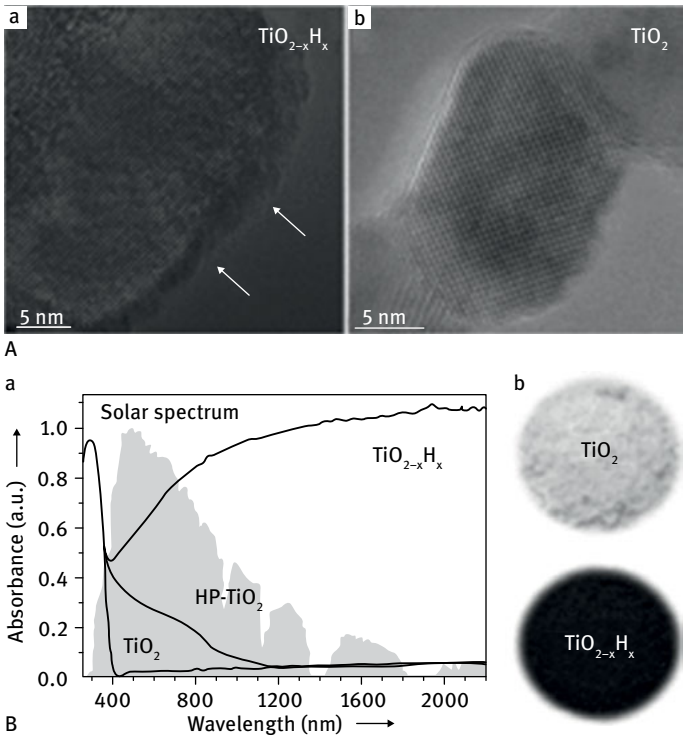

Fig. 4.16: "Black" TiO_2 nanoparticles. **A:** Electron microscopy images showing an amorphous layer (indicated by the arrows) presumably corresponding to hydrogenated TiO_2 formed around the crystalline TiO_2 nanoparticle core. **B:** Physical appearance of the TiO_2 nanoparticles (right), and a graph showing the enhanced absorbance of visible and infrared light by hydrogenated (black) TiO_2 nanoparticles. The wavelength range of the solar spectrum is shown in grey. Reprinted with permission from Wang et al., *Adv. Funct. Mater.* **23** (2013), 5444–5450, © 2013 John Wiley and Sons.

light absorption in the visible and infrared regions of the electromagnetic spectrum (Fig. 4.16B).

Photocatalysis, mostly aimed at efficient decomposition of organic pollutants, is a broad and commercially viable application in which TiO_2 NPs have played a central role due to their low cost, efficiency, and benign environmental impact. The mechanism of photocatalytic reactions induced by TiO_2 (and other semiconductors for that matter) is shown in Figure 4.17. Electrons are excited by light from the valence band to the conduction band; the photo-excited electrons (and the holes formed simultaneously in the valence band) can subsequently react with molecular species adsorbed onto the NP surface – electron acceptors can react with the electrons in the conduction band, electron donors with the holes in the valence band – resulting in chemical transformation/decomposition of the adsorbed species. This process can be a powerful means for degrading various organic pollutants adsorbed onto the TiO_2 NP sur-

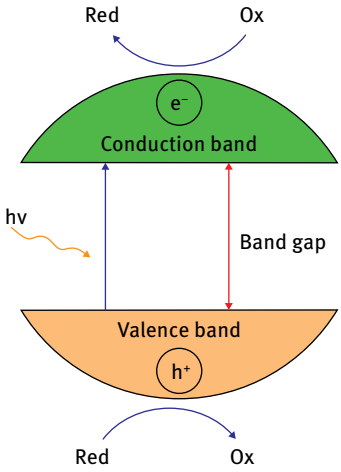

Fig. 4.17: Photocatalysis by TiO_2 nanoparticles. The energy diagram shows the physical/chemical events: photoexcitation of the electrons and subsequent redox reactions with adsorbed species.

face. The main advantage of using TiO_2 nanoparticles as photocatalysts is the significantly large surface area they provide for adsorption and interaction with the desired reactants.

TiO_2 NP photocatalysis has been aided by modifications to the NP synthesis processes. In some cases, doping the TiO_2 NPs with metal ions has been shown to enhance the catalytic activity, presumably by reducing the rate of electron-hole recombination (which minimizes charge transfer to the NP-adsorbed target molecules). Nonmetallic dopants, such as nitrogen or sulfur atoms, were also found to contribute to the photocatalytic properties of TiO_2 NPs. Those dopants are believed to stabilize reaction intermediates at the NP surface, as well as "trap" holes in the semiconductor's valence band and thus inhibit electron-hole recombination, similar to the aforementioned effect of metal dopants.

Water splitting (i.e. decomposing water to O_2 and H_2) is considered one of the most sought after "holy grails" in TiO_2-induced photocatalysis, due to the enormous potential of *hydrogen* as a clean energy source in fuel cells. The generation of O_2 and H_2 by photocatalysis is shown in Figure 4.18A. Essentially, photons with the same or larger energy than the semiconductor bandgap generate electrons and holes; the electrons in the conduction band can reduce the hydrogen in water, yielding H_2, while the holes in the valence band oxidize the oxygen atoms to produce O_2. Various TiO_2 NP structures have been investigated as water-splitting catalysts. Similar to the dye-sensitized nanoparticles discussed above, experimental schemes have explored doping the TiO_2 NPs in order to expand the energy absorbance range. Figure 4.18B, for example, shows TiO_2 nanowires decorated with *gold* nanoparticles, synthesized by Y. Li and colleagues at the University of California, Santa Cruz, which exhibited enhanced water-splitting photocatalysis. The exact mechanism for the Au-induced amplified catalytic properties has not been elucidated, the effect is believed to occur

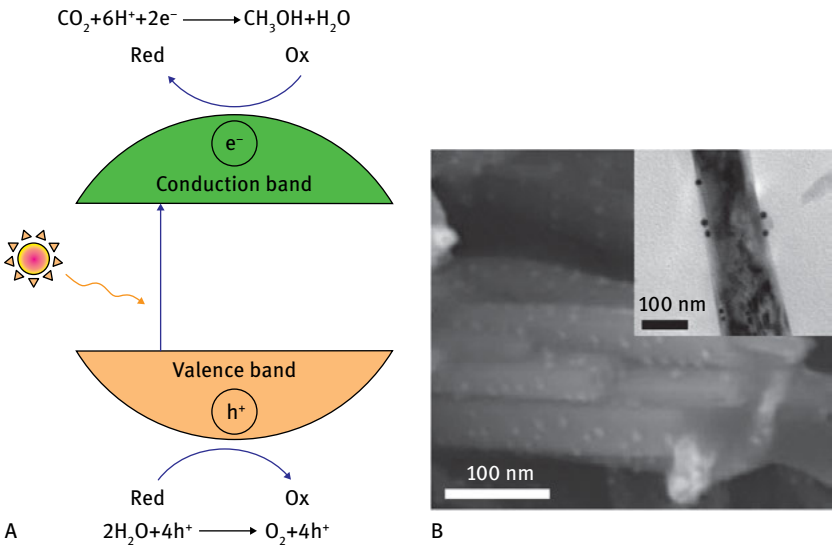

Fig. 4.18: Photocatalysis of the water splitting reaction achieved by TiO_2 nanoparticles. **A:** Energy level diagram depicting the redox reactions induced by the photo-excited electron and hole, respectively. **B:** Electron microscopy image showing TiO_2 nanowires decorated with gold nanoparticles (shown as white specks) used as a water splitting catalyst. Reprinted with permission from Pu et al., *Nano Lett.* **13** (2013), 3817–3823, © 2013 American Chemical Society.

via generation of high-energy surface electrons on light irradiation of the Au NPs, which can subsequently be transferred to the TiO_2 and enhance catalysis of the water splitting reactions.

Hydrogen storage research is closely related to water splitting – both aiding the fledgling efforts towards a future "hydrogen economy". Specifically, storing the hydrogen gas generated in water splitting processes (or in other chemical reactions) is considered a major technical challenge. TiO_2 NPs are particularly amenable for hydrogen storage as they exhibit a very large surface area, are known to efficiently adsorb gas molecules, and are generally stable in different environmental conditions. Figure 4.19 presents experimental results reported by J. Lin and colleagues at the National University of Singapore, demonstrating that elongated TiO_2 nanotubes exhibited significantly higher nitrogen gas adsorption compared to the bulk material, confirming the significance of the expanded surface area of TiO_2 NPs in potential hydrogen storage applications.

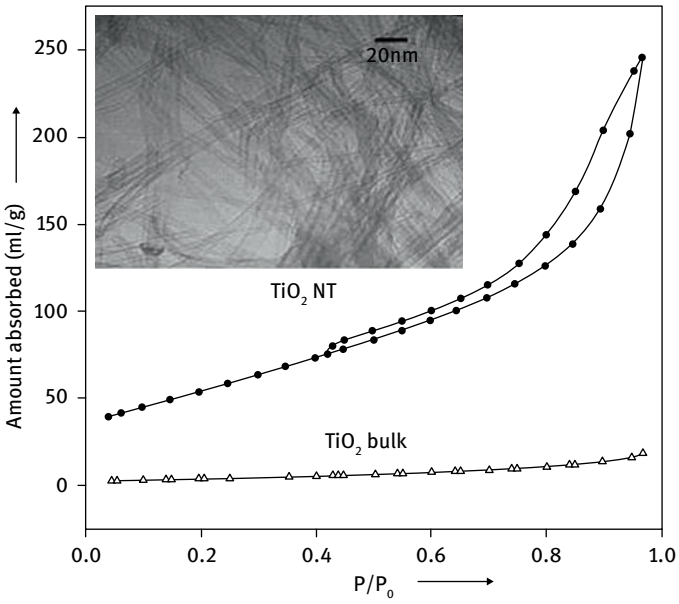

Fig. 4.19: Enhanced gas adsorption on TiO_2 nanotubes. Higher gas adsorption recorded in the TiO_2 nanotube samples (solid circles) compared to bulk TiO_2 (empty circles). The inset shows an electron microscopy image of the nanotubes. Scale bar corresponds to 20 nm. Reprinted with permission from Lim et al., *Inorg. Chem.* **44** (2005), 4124–4126, © 2005 American Chemical Society.

4.3 Zinc oxide nanoparticles

Zinc oxide (ZnO) is used in many industrial applications, primarily as a stabilizer and additive in rubbery materials, ceramics, ointments, and foods. ZnO is a wide bandgap semiconductor, and similar to TiO_2 has been employed in photocatalysis and related applications. ZnO nanoparticles frequently exhibit properties superior to other semiconducting NPs, specifically high chemical and physical stability, low cost, nontoxicity, efficient energy absorbance and light emission, and good electron transport. Representative applications of ZnO NPs are summarized below.

Synthesis of ZnO NPs is usually carried out in nonaqueous (organic) solutions by reacting zinc ions with water (i.e. hydrolysis) at high temperatures. Like other NP systems, amphiphilic protective agents are added to the reaction mixtures to stabilize the resultant NPs and prevent their aggregation. Various reaction parameters have been found to affect ZnO NP sizes and morphologies. Figure 4.20 shows monodisperse ZnO NPs of different morphologies synthesized by R. Brayner and colleagues at Universite Paris Diderot, France, by variation of the ratio between the water molecules and the Zn^{2+} ions in the reaction mixtures (i.e. the "hydrolysis ratio").

Research focusing on ZnO nanorods (NRs) is a particularly active field, since NRs have been found in many instances to exhibit better physical properties than their

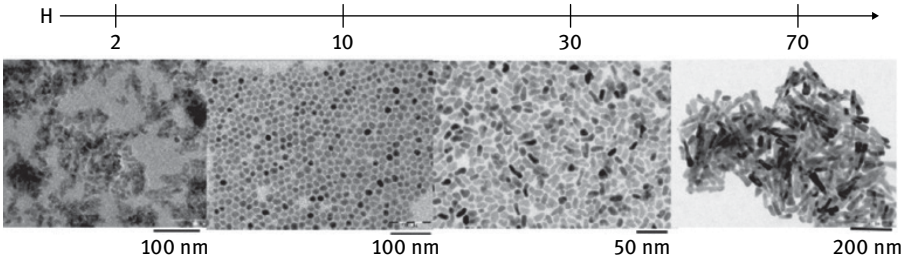

Fig. 4.20: Uniform ZnO nanoparticles of distinct shapes and sizes. Control of nanoparticle structure was achieved by modulation of the hydrolysis ratio ($H = n_{H2O}/n_{Zn2+}$). Reprinted with permission from Brayner et al., *Langmuir* **26** (2010), 6522–6528, © 2010 American Chemical Society.

spherical ZnO NP counterparts. ZnO NRs (and by extension nanowires) are mainly synthesized via directed growth initiated by surface-attached *nucleating sites* (ZnO NPs or gold NPs). Various substrates have successfully been employed as surfaces for ZnO NR growth. Figure 4.21 portrays ZnO nanorods and "nanoneedles" grown on the surface of *cotton fibers*. Specifically, R. R. Ozer and colleagues at the University of Tulsa, Oklahoma, have shown that NR morphologies and dimensions could be modulated by tuning the ratio between the concentrations of the nanoparticle "seeds" and the ZnO precursors in the growth solution.

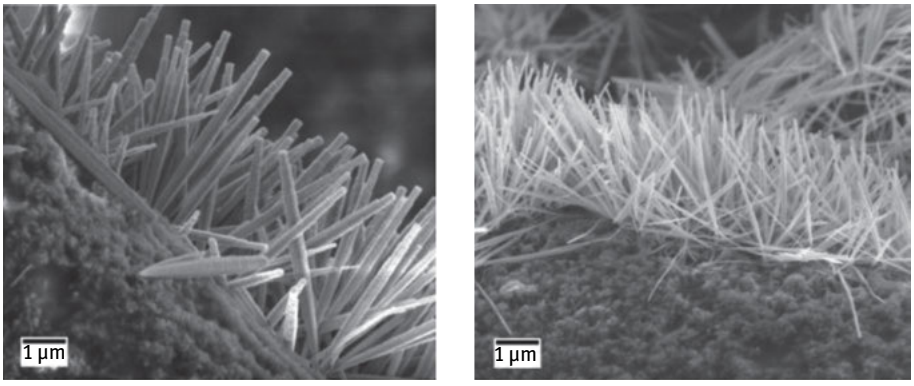

Fig. 4.21: ZnO nanorods and "nanoneedles". ZnO nanostructures grown on the surface of cotton fibers. Nanorod morphology and dimensionalities are linked to the ratio between the concentrations of the nucleation seeds and nanorod growth-reagents: **A:** seed-to-growth reagents with a ratio of 2; **B:** seed-to-growth reagents with a ratio of 4. Reprinted with permission from Athauda et al., *ACS Appl. Mater. Inter.* **5** (2013), 6237–6246, © 2013 American Chemical Society.

Laser emission has been one of the unique physical phenomena recorded for ZnO NRs (for more in-depth discussion of the lasing properties of semiconductor nanorod lasers see Chapter 2). Practical utilization of ZnO "nanolasers", however, is limited if one aims to utilize single nanorods, and would rather be aided by macro-scale ordering and alignment of NR populations. Figure 4.22 depicts an ordered ZnO NR array displaying dramatic lasing properties. The vertically aligned and uniform NRs were produced by H. Zhou and colleagues at Universitaet Karlsruhe, Germany, by a chemical vapor deposition (CVD) technique employing patterned polymer (polystyrene) nanospheres as nucleating seeds. The ZnO NR assembly shown in Figure 4.22 generated high intensity and sharp lasing emission peaks upon photo-excitation, attesting to the potential practical applications of the material.

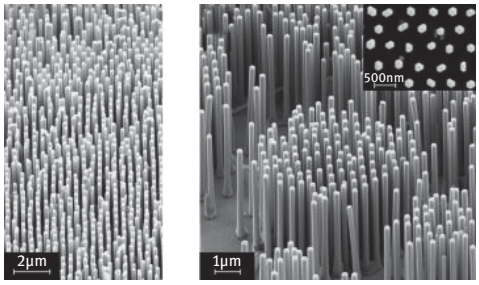

Fig. 4.22: ZnO nanorod array exhibiting lasing properties. Side-views (**A–B**) and top view (*inset*) of the ZnO nanorods grown vertically upon the substrate. The nanorod array produced intense lasing upon excitation. Reprinted with permission from Zhou et al., *Appl. Phys. Lett.* **91** (2007), 181112, © 2007 American Institute of Physics.

Like other semiconductor NPs, ZnO NPs have been widely used in photocatalysis. As discussed above in the case of TiO_2 NPs, photocatalytic reactions involving substances adsorbed onto the NP surface occur through light excitation in wavelengths corresponding to (or exceeding) the semiconductor bandgap; the electrons photo-excited from the valence band to the conduction band (and/or the holes simultaneously formed in the valence band) could react and induce decomposition of the NP-adsorbed species. ZnO, in fact, exhibits excellent *quantum efficiency* (i.e. efficiency at converting absorbed photons into electrons), and as such has often displayed better photocatalytic properties than other commonly used catalysts, such as TiO_2 NPs.

A distinct disadvantage of ZnO in the context of photocatalysis is its bandgap, which is not wide enough to cover parts of the ultraviolet spectral range in sunlight, thus reducing the overall catalytic efficiency of the material. Doping ZnO NPs with other atoms, particularly metal ions, has been successfully employed to overcome this limitation. Mg^{2+} doping, for example, was shown to enhance light absorption and photocatalytic efficiency by increasing the bandgap of ZnO NPs. This phenomenon is thought to occur because some of the zinc ions in the ZnO crystal lattice are substituted with magnesium (noting that the energy gap of MgO is significantly higher than that of ZnO). Studies have demonstrated that ZnO NPs doped with other ions also exhibited higher photocatalytic performance. Metal doping of ZnO NPs gave rise to other inter-

esting physical phenomena. *Aluminum* doping of ZnO NPs, for example, was found to induce plasmon resonance absorbance of infrared (IR) light. The proposed mechanism for this intriguing observation was that the substitution of zinc ions in the ZnO NP lattice with aluminum generated free electrons, which consequently gave rise to light absorption through surface plasmon resonance arising from oscillation of the partly-anchored electrons on the doped ZnO NP surface.

ZnO NPs have been recently examined as ingredients in *sunscreen* lotions. The sun blocking action of ZnO (as well as TiO_2) is related to the relatively significant absorbance of ultraviolet light (due to the wide bandgap of this semiconductor). While a practical limitation for the use of many semiconductor materials in sunscreens is their *opaqueness*, the use of nanoparticles might mitigate this problem, significantly increasing the transparency of the manufactured lotions. The increased use of ZnO NPs in sunscreens (and in other cosmetics and consumer products) has led, however, to heightened awareness and discussion of the biological risks of the material, as NPs can penetrate the skin easily and thus might interfere with various physiological processes (see Chapter 7 for an in-depth discussion of the biological and cellular implications of nanoparticles). In the case of ZnO NPs there are indeed reasons for concern, primarily due to the relatively low stability of ZnO in aqueous solutions, resulting in its dissolution to zinc and oxide ions. While Zn^{2+} is normally present in the body and is involved in numerous biochemical processes, elevated levels of this ion (which might be locally incurred through dissolution of ZnO NPs) might be toxic. Indeed, several studies have pointed to toxic effects associated with high Zn^{2+} concentrations induced through cell uptake of ZnO NPs and their intracellular dissolution.

Another potential toxic factor associated with ZnO NPs in close proximity with cells and tissues is the generation of *radicals* – atomic and molecular species containing *unpaired* electrons. Radicals are widely believed to contribute to toxic processes in cells and tissues, primarily involving oxygen atoms (usually referred to as reactive oxygen species, ROS). While radicals also participate in natural metabolic and signaling processes, ROS have been implicated as toxic agents in various diseases and pathologies – in which toxicity was attributed to the high reactivity of the radicals. In this context, electrons released by photo-excited ZnO NPs might be transferred to biological molecules, generating harmful ROS. Overall, the biological risks associated with ZnO NPs require further research.

4.4 Silicon oxide nanoparticles

Silicon oxide (SiO_2) has been utilized by mankind for thousands of years. This substance is abundant in nature, most notably as quartz and other minerals in bones and microorganism shells. SiO_2 is the basic building block of widely-used materials including glass, ceramics, optical fibers, and others. Silicon has been also part of the "nanorevolution", largely through introduction of "nanoporous" silicon-based mate-

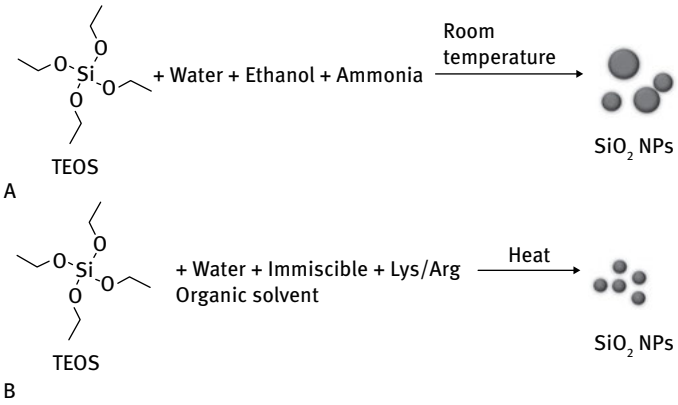

Fig. 4.23: Reaction schemes for synthesis of SiO_2 nanoparticles. **A:** The "Stöber process", generating relatively large nanoparticles. **B:** Reaction pathway using basic amino acids, for fabrication of smaller SiO_2 nanoparticles.

rials used as catalysts, molecular sieves, and in drug delivery. This section focuses on SiO_2 nanoparticles, emphasizing their useful physico-chemical properties, biocompatibility, and applications.

Different solution-phase synthesis routes for the fabrication of SiO_2 NPs have been developed. The "Stöber process", shown in Figure 4.23A, is one of the most widely implemented. In this process, the SiO_2 precursor tetraethyl orthosilicate (TEOS) is treated with ammonia (acting as a catalyst) in a solvent mixture of water and ethanol. The reaction proceeds in two steps. First, TEOS undergoes hydrolysis, in which the organic ligands bound to the silicon are removed by reaction with water molecules, followed by condensation to form the -Si-O-Si network comprising the skeleton of the SiO_2 NPs. The particles formed via this pathway are usually relatively large (>100 nm); smaller SiO_2 NPs can be synthesized by using basic amino acids such as arginine or lysine as stabilizers within an immiscible organic solvent. Subsequent hydrolysis and condensation of TEOS produces SiO_2 NPs with diameters of as low as 10 nm (Fig. 4.23B).

Significant research into SiO_2 NP properties and applications has been carried out at the interface between nanotechnology and biology, primarily due to the biocompatibility and perceived lack of toxicity of these NPs. Further aiding their biological applicability is the observation that the relatively porous matrix of SiO_2 NPs facilitates the loading of molecular guests. In addition, the SiO_2 surface can also be covalently functionalized – enabling display of recognition and targeting residues. These properties have been widely exploited in biological imaging applications. Figure 4.24 portrays applications of *fluorescent* SiO_2 NPs for cell and tissue imaging. The imaging system, designed by K. Wang and colleagues at Hunan University, China, comprised of SiO_2 NPs encapsulating fluorescent dye molecules. The researchers demonstrated cell uptake of the SiO_2 NPs, making visualization of the cells using fluorescence mi-

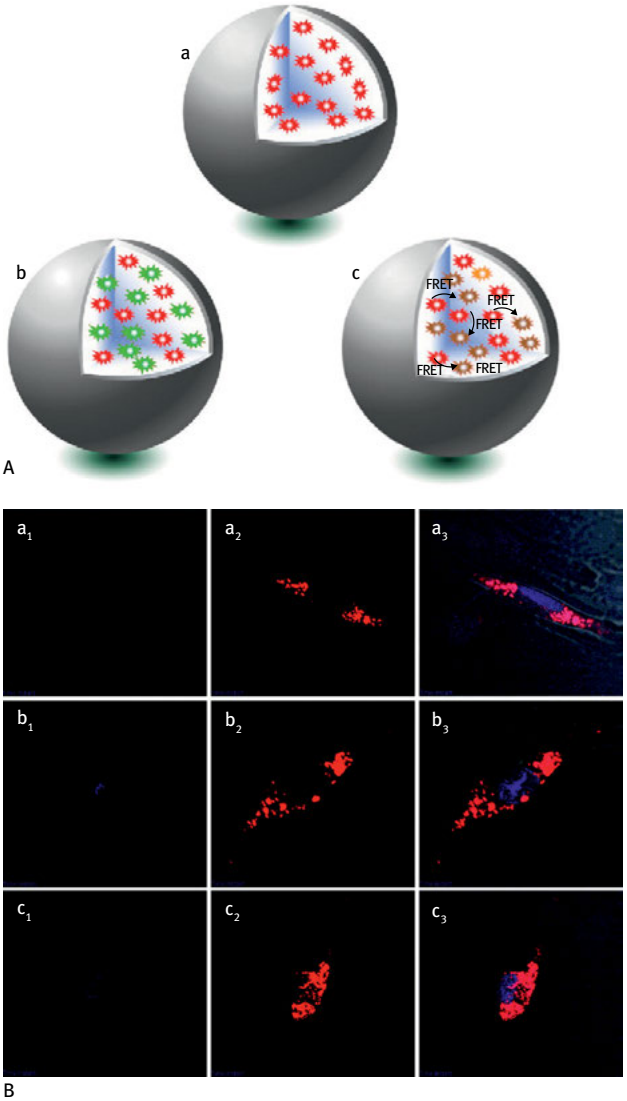

Fig. 4.24: SiO_2 nanoparticles encapsulating fluorescent dyes and their use in cell imaging. **A:** Schematic depiction of the nanoparticles containing: a. single fluorescent dye; b. a mixture of two dyes; and c. two dyes between which energy can be transferred by a Forster resonance energy transfer (FRET) process. Reprinted with permission from Wang et al., *Acc. Chem. Res.* **2013** *46*, 1367–1376, copyright (2013) American Chemical Society. **B:** Cell imaging using fluorescently-labeled SiO_2 nanoparticles. The panels in **a** correspond to images recorded after 24 hours of incubation; **b** – 48 hours; **c** – 72 hours. Left column: labeling with a nucleus-specific fluorescent dye; middle column: fluorescence emission of the dye-hosted SiO_2 nanoparticles; right column: combined images. The fluorescence microscopy data confirm internalization of the SiO_2 nanoparticles within the cells. Reprinted with permission from Liu et al., *Bioconjugate Chem.* **21** (2010), 1673–1684, © 2010 American Chemical Society.

croscopy possible. Notably, SiO_2 NPs can host more than a single fluorescent dye and also dye mixtures, permitting *multicolor* imaging capabilities. Moreover, pairs of dyes exhibiting energy transfer between them can be encapsulated together within a single NP – an important feature enabling greater flexibility in the choice of excitation wavelengths employed (often a critical issue in physiological and tissue environments) to achieve optimal imaging capabilities.

Mesoporous SiO_2 nanoparticles (MSNs) have attracted significant interest as a promising vehicle for biological applications. MSNs belong somewhat to the "mesoscale" world, as their sizes in most cases are in the range of hundreds of nanometers, however they still merit discussion in the context of this section in light of their chemical and biological properties which are dependent on their nanoscale characteristics. The defining feature of MSNs is their *porosity* – providing substantial internal surface area and volume, and thus making the particles available to load large quantities of molecular cargoes. MSNs have additionally been promoted as an effective platform for delivery of biological and therapeutic substances to cells and tissues because of the diverse chemical functionalization routes of the SiO_2 framework and its biocompatibility. Furthermore, the porous morphology could provide a "shielding mechanism", protecting the embedded molecular guests from physiological degradation as the NPs are transported to the site of action inside the body.

MSNs in have been examined as conduits for *gene delivery*, a highly sought, albeit challenging therapeutic goal. Figure 4.25 illustrates two distinct gene-transport MSN systems prepared by D-H Min and colleagues at the Korea Institute of Science and Technology. The researchers created two types of MSNs, comprising of small and large pores, respectively, and coated them with a layer of positive residues, designed to bind DNA molecules through electrostatic attraction. Interestingly, the MSNs exhibiting small, nanometer-scale pores were less effective gene carriers, since the DNA molecules could not enter the pores, adsorbed instead upon the MSN surface and degraded by DNA-digesting enzymes before reaching their cellular targets. However, when the MSNs had larger pores, gene delivery was more successful due to protection of the DNA molecules inserted deep within the silica pores (Fig. 4.25B).

Figure 4.26 depicts other MSN morphologies. These NPs were prepared by C. J. Brinker and colleagues at the University of New Mexico via a synthetic method termed "evaporation-induced self-assembly" (EISA). This technique involves mixing an SiO_2 precursor with amphiphilic surfactants; the surfactant/SiO_2 constituents self-assemble into small spherical structures (i.e. "micelles") upon slow evaporation of the solvent, ultimately producing organized mesoporous NP structures. Inclusion in the reaction mixtures of different surfactants in different mole ratios yielded diverse morphologies, such as "onion-shaped" lamellar structures and domain formation within the MSNs.

A central issue in MSN research concerns devising mechanisms for controlled release of the molecular cargo transported within the particles when they reach their physiological targets. Numerous strategies have been developed to achieve this goal

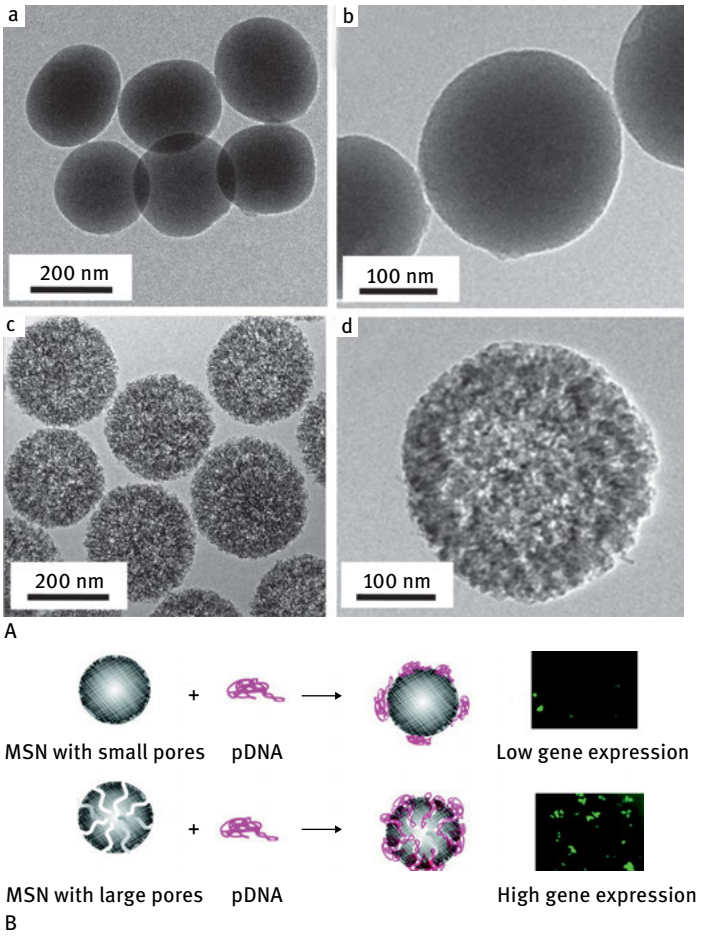

Fig. 4.25: Mesoporous silica nanoparticles (MSNs) for gene delivery. **A:** Electron microscopy images showing MSNs exhibiting small pores (and corresponding smooth surface area, **a–b**), and "swelled" MSNs containing larger pores (**c–d**). **B:** Illustration showing usage of the two MSN types for drug delivery. The small-pore MSNs do not allow insertion of DNA molecules, which instead are attached to the particle surface whereby they are enzymatically degraded. The large-pore MSNs allow encapsulation of the DNA deeper within the particle. The DNA molecules are thus more protected, giving rise to efficient delivery. Reprinted with permission from Kim et al., *ACS Nano* **5** (2011), 3568–3576, © 2011 American Chemical Society.

and only a few examples can be discussed here; in general, chemical modification of MSNs has been the preferred approach for endowing controlled release capabilities to the particles. Key aspects of controlled release mechanisms include the choice of external stimuli triggering release, feasibility and efficiency of the release processes in actual physiological scenarios, and the extent of target selectivity.

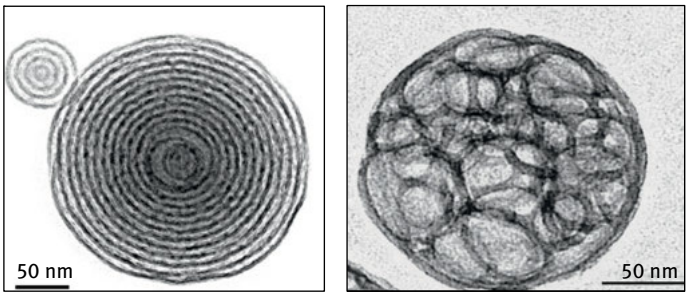

Fig. 4.26: Mesoporous silica nanoparticles. Electron microscopy images showing distinct morphologies produced via evaporation-induced self-assembly (**A**), and solution-based self-assembly (**B**). The strikingly different nanoparticle organizations were ascribed to the presence of different surfactants and reactant concentrations. Reprinted with permission from Tarn et al., *Acc. Chem. Res.* **46** (2013), 792–801, © 2013 American Chemical Society.

Figure 4.27 depicts an elegant MSN system in which temperature increase was the triggering event for cargo release. The "tailor-made" particles, produced by R. Martinez-Manez and colleagues at the Universitat de Valencia, Spain, were functionalized with an amphiphilic molecule (alkylsilane), which in turn enabled further coating of the particles with a hydrophobic paraffin layer (Fig. 4.27A). When the temperature was increased to above the melting point of paraffin, the hydrophobic paraffin capping layer disintegrated, releasing the entrapped guest molecules. To demonstrate the therapeutic potential of the triggering mechanism, the researchers released a MSN-embedded fluorescent dye within living cells through raising the temperature from 37 °C to 42 °C (Fig. 4.27B).

Acidity (e.g. *pH change*) has been another external stimulus for controlled release of therapeutic cargo from MSNs. pH is, in fact, a pertinent parameter for targeted delivery applications because acidity varies both among different tissues as well as in disease conditions. In particular, it is known that cancer cells induce higher acidity in their environment – thus opening the way for possible therapeutics through pH-triggered controlled release of drugs in tumor areas. Moreover, another fundamental physiological parameter underlying pH-based release mechanisms has been the realization that MSNs (like many other foreign substances) enter the cells via transport to the *lysosomes* (i.e. *endocytic pathways*), which exhibit high internal acidity. Accordingly, pH-sensitive release would be an efficient cell-targeting approach, since the pH outside the cell (e.g. in the bloodstream) is neutral.

Figure 4.28 illustrates such a pH-based release mechanism in which proteins adsorbed within MSN pores were delivered across cellular membranes and then released inside the cell. In the experimental scheme, demonstrated by V. S. Y. Lin and colleagues at the Iowa State University, a representative enzyme (cytochrome-C) was encapsulated in the MSN pores by electrostatic interactions between the enzyme and

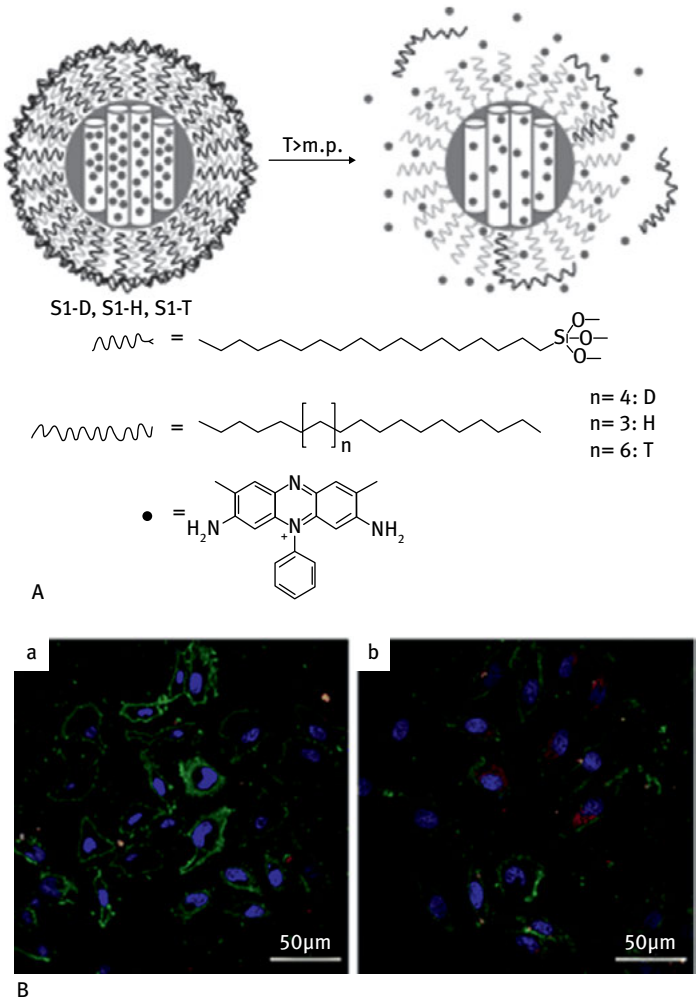

Fig. 4.27: Temperature-triggered release mechanism of molecular cargo within mesoporous silica nanoparticles. **A:** The experimental scheme: mesoporous silica nanoparticles encapsulating a fluorescent dye (depicted as black circles and representing a molecular guest) are coated with a hydrophobic layer (alkylsilane) and paraffin. On increasing the temperature the paraffin cap disintegrates, resulting in release of the fluorescent dye. **B:** Confocal fluorescence microscopy images showing temperature-triggered intracellular release of a fluorescent dye modeling a guest cargo. **(a)** 37 °C – no release of the red fluorescent dye; **(b)** 42 °C – the dye is released inside the cells, resulting in red staining of the intracellular space. The cell nuclei are stained by a blue dye to help identify cell positions, and a green dye marks the plasma membrane of the cells. Reprinted with permission from Aznar et al., *Angew Chem.* **123** (2011), 11368–11371, © 2011 John Wiley & Sons.

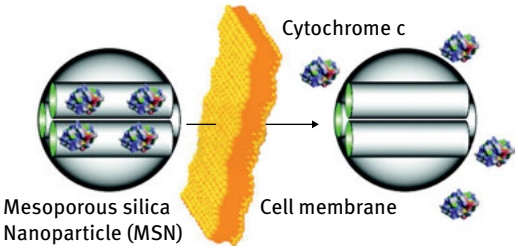

Fig. 4.28: pH-triggered release from mesoporous silica nanoparticles. Cytochrome-C molecules are embedded within the nanoparticle pores by electrostatic attraction. Acidic pH in the intracellular compartments minimizes the electrostatic interactions, resulting in release of the encapsulated cytochrome-C guest molecules. Reprinted with permission from Slowing et al., *JACS* **129** (2007), 8845–8849, © 2007 American Chemical Society.

pore walls. Importantly, the difference between the (neutral) pH in the extracellular space and the acidic pH within cell compartments associated with cell transport (i.e. endosomes, lysosomes) led to a change in the electrostatic charge on the MSN surface. As a consequence, the attraction between the enzyme molecules and the MSN pores became weaker, thereby triggering their release. The study highlighted in Figure 4.28 is additionally noteworthy because it demonstrates that MSNs could be an effective platform for delivering biological molecules *across physiological barriers* (i.e. the cell membrane).

A somewhat more complex system demonstrating a pH-triggered release is depicted in Figure 4.29. The design concept, developed by J. I. Zink and colleagues at the University of California, Los Angeles, is based on the display of pH-sensitive "molecular rods" on the MSN surface. The rods comprised of an elongated carbohydrate chain displaying positively-charged amine residues at two locations close to the rod "base", and a nitrogen atom close to the rod terminus which can be *protonated*, depending on the pH of the solution (Fig. 4.29A). As shown in Figure 4.29, the rods attached to the pore surface were further partly coated with pumpkin-shaped "molecular beads" which, importantly, were negatively-charged. Accordingly, in neutral pH the beads were located at the lower ends of the rods – electrostatically attached to the positive amine residues. In this configuration the bulky beads inhibited release of the entrapped substance, as they were positioned right at the MSN surface blocking the pore "exits" to the solution. However, in (slightly) acidic environments, the nitrogen at the top of the rod became protonated and thus positively-charged; the negative beads were consequently repositioned and moved towards the charged nitrogen, "opening" the pores and allowing cargo release.

Enzyme-triggering is a popular controlled-release mechanism in MSNs, primarily because of its intrinsic specificity (through enzyme-substrate recognition) and biological relevance. Figure 4.30 illustrates such an enzyme-triggered release system, in which the MSNs were functionalized with chemical moieties which could be

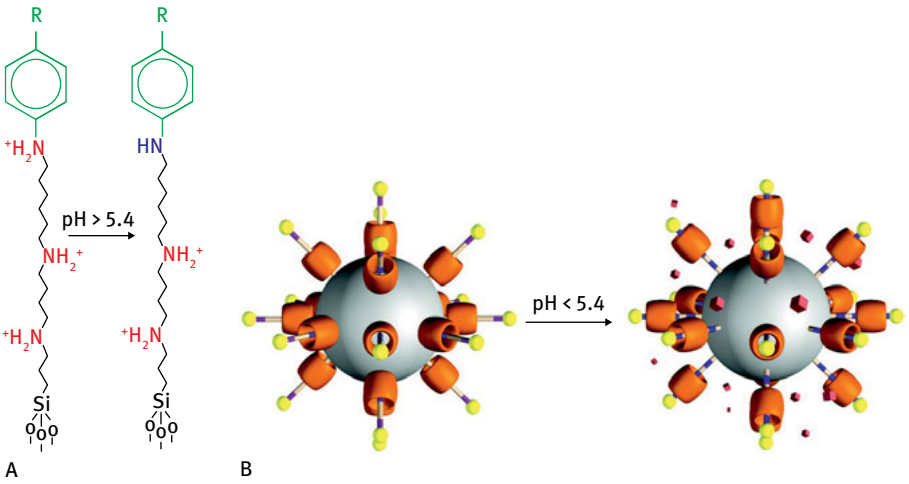

Fig. 4.29: pH-triggered release of cargo from mesoporous silica nanoparticles by a "molecular motion" mechanism. **A:** Structure of the molecular rod; note in particular protonation of the nitrogen close to the aromatic moiety in low pH. **B:** Schematic depiction of the pH-release mechanism. In neutral pH (*left*) the negatively-charged "beads" (shown in orange) placed around the molecular rods (displaying the yellow tips) are located close to the nanoparticle surface, thereby blocking cargo release from the nanoparticle pores. In acidic pH (*right*) the top nitrogen within the molecular rods is protonated, pulling the beads "upwards", thereby unblocking the pores and releasing the cargo. Reprinted with permission from Angelos et al., *JACS* **131** (2009), 12912–12914, © 2009 American Chemical Society.

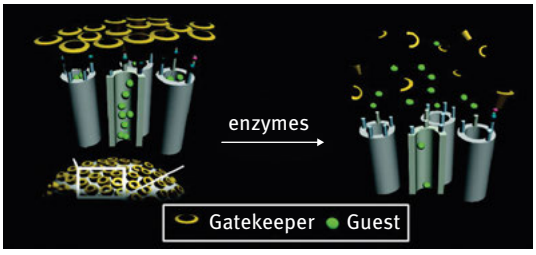

Fig. 4.30: Enzyme-triggered release of molecular guests within mesoporous silica nanoparticles. Cyclodextrin (CD) residues (shown as yellow rings) are attached to the nanoparticle surface blocking the pores and preventing release of the encapsulated cargo (left). Enzyme catalysis degrades the CD "gatekeepers", resulting in pore opening and cargo release. Reprinted with permission from Park et al., *JACS* **131** (2009), 16614–16615, © 2009 American Chemical Society.

recognized (and digested) by enzymes. Specifically, C. Kim and colleagues at Inha University, Korea, functionalized the porous surface of the MSNs with cyclodextrin (CD) moieties. CD is a bulky, toroid-shaped sugar residue acting in this system as a "gate-keeper", preventing release of the MSN-encapsulated guest molecules. The researchers, however, showed that two common enzymes could react with the CD-

functionalized MSNs, degrading the CD "pore-blockers" and inducing release of the embedded molecules: *amylase* which specifically binds and hydrolyzes cyclodextrin, and *lipase* which recognizes and cleaves ester bonds (present here within the "arm" connecting the CD to the MSN surface).

Light activation is another external triggering strategy for controlled release of MSN-entrapped molecules. Figure 4.31 portrays such a mechanism. This MSN assembly, designed by J. I. Zink and colleagues, was functionalized with light-sensitive *azobenzene* molecules. The "azo" unit (benzene ring attached to the N=N bond; see Fig. 4.31) undergoes back-and-forth transformations between the "cis" and "trans" positions when illuminated (i.e. *photo-isomerization*). Initially, the azo-containing molecules covalently attached to the MSN surface (and close to the pore opening) do not allow passage of the encapsulated molecules. However, while the bulky benzene residues constitute effective blockers of the MSN pores, their light-induced flipping (or "wagging") allowed slow release of guest molecules.

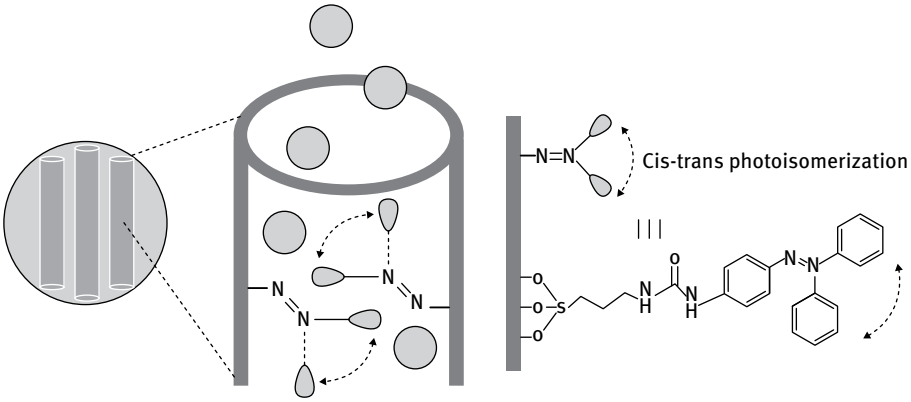

Fig. 4.31: Light-activated release of encapsulated guests in mesoporous silica nanoparticles. The azo-containing residues initially block the pore entrance, preventing cargo release. Light-induced flipping of the azo unit (the benzene ring) enables passage of encapsulated guests and their release from the pores. Reprinted with permission from Lu et al., *Small* **4** (2008), 421–426, © 2008 John Wiley & Sons.

Despite the perceived nontoxicity of SiO_2 NPs, considerable research has been carried out with the goal of assessing their cellular impact and biological safety. Indeed, concerns have been raised regarding the long-term physiological effects of SiO_2 NPs. *Silicosis*, in particular, is a debilitating lung disease associated with exposure to SiO_2 dust. There have been, however, no studies demonstrating a definitive causative link between silicosis and SiO_2 NPs. Other risk factors need to be considered as well. Based on in vitro studies, it is believed that SiO_2 NPs might induce cell membrane damage through electrostatic affinity between negatively-charged domains within the SiO_2

framework (such as SiO^-) and positive moieties in membranes (for example the abundant choline unit in many phospholipids comprising membrane frameworks).

While the majority of reported applications of SiO_2 NPs have been biological, other potential uses have been proposed, taking advantage of the hosting capabilities of the particles. An intriguing application of SiO_2 NPs as a conduit for *white light generation* is shown in Figure 4.32. Fabrication of white light emitters (also referred to as "white fluorescence" emitters) is, in fact, quite a challenging task for chemists. Essentially, white light emitters include (at least) three different dyes producing blue, green, and orange (or yellow) light, respectively; mixing the three dyes yields white light. The dye concentrations and physical distributions of the emitters need to be carefully optimized to achieve a balanced white light and prevent photophysical processes such as energy transfer among the dye molecules. SiO_2 NPs constitute, in principle, an excellent platform for white light generation due to their intrinsic transparency and the possibility of encapsulating different guest molecules within the same particle.

The white light emitting system designed by P. Audebert and colleagues at the Ecole Normale Superieur de Cachan, France, consisted of SiO_2 NPs doped with two fluorescent dyes of distinct colors: *naphthalimide* (blue) and *tetrazine* (yellow-orange). Importantly, the researchers showed that changing the mole ratio between the two dyes encapsulated within the SiO_2 NPs and tuning the preparation protocols generated three colors: blue (free naphthalimide), green (naphthalimide forming excited dimers, or "excimers" within the NPs), and yellow/orange (tetrazine bound to the NP surface). As demonstrated in Figure 4.32, different emission colors including white light could be produced from SiO_2 NPs of different dye combinations.

Encapsulation of fluorescent dyes within SiO_2 NPs has been carried out via other means, producing composite SiO_2 NPs exhibiting interesting photophysical properties. Figure 4.33, for example, outlines an elegant method for synthesis of dye/SiO2 core-shell NPs exhibiting extremely bright and tunable fluorescence. The two-step synthesis procedure, developed by U. Wiesner and colleagues at Cornell University, was based on forming the NP "core" using SiO_2 precursors which were covalently attached to the desired fluorescent dye; the "shell" was subsequently assembled by conventional NP growth processes, such as the Stöber route (Fig. 4.23, above). The NPs produced using this approach exhibited excellent stability and brightness ascribed to immobilization of the fluorophore within the SiO_2 core and the shielding effect of the shell. Furthermore, as demonstrated in Figure 4.33, the technique allowed encapsulation of diverse dyes within the NPs, forming NPs exhibiting a broad range of colors.

4.5 Rare earth oxide nanoparticles

Rare earth elements have electrons in the *f orbitals* which are relatively far from the nucleus, endowing the atoms with distinct physico-chemical properties. Rare earth *oxides* (oxygen-containing molecules of *lanthanides*, *scandium*, and *yttrium*) have

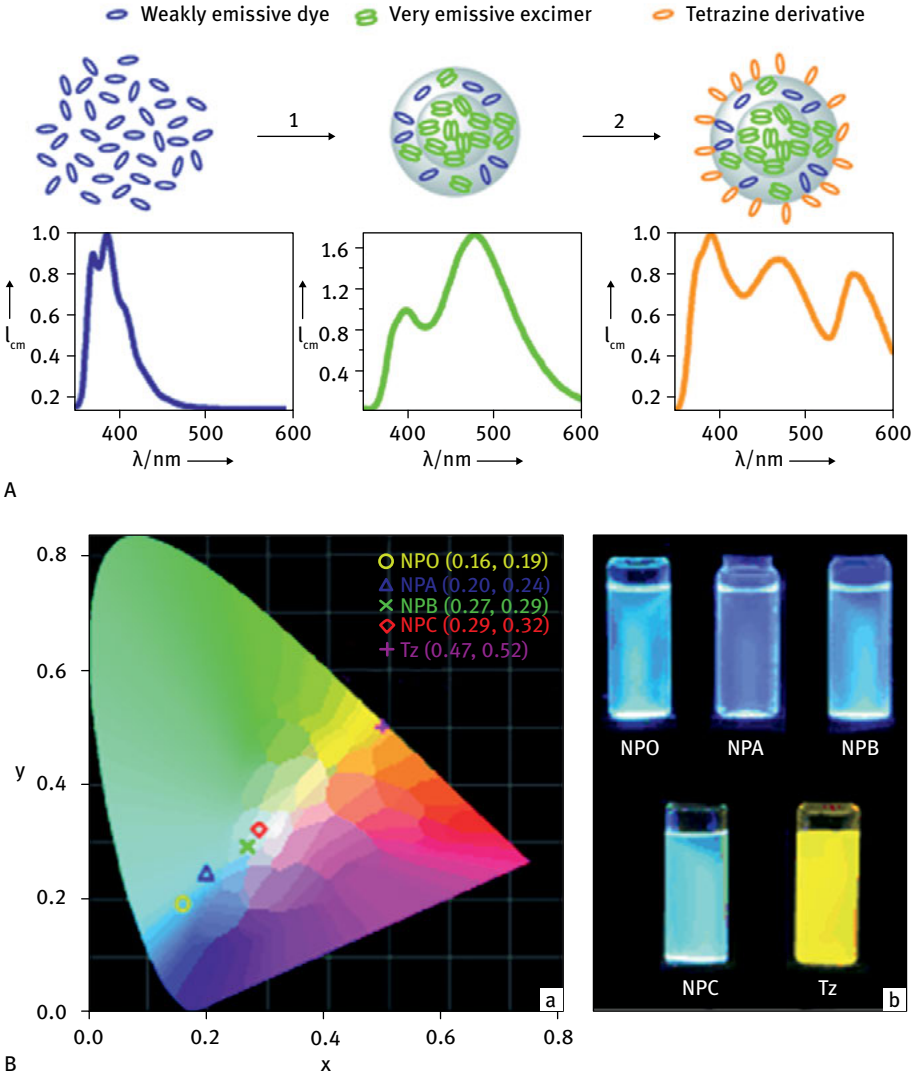

Fig. 4.32: Silicon oxide nanoparticles form a white light emitter. Different colors generated by association of two fluorescent dyes within SiO_2 nanoparticles. **A:** Schemes of the dye/nanoparticle assemblies and corresponding emission spectra (i.e. colors): nanoparticle-free naphthalimide (blue); naphthalimide embedded within the SiO_2 nanoparticles forming excimers (green); tetrazine bound on the SiO_2 nanoparticle surface (yellow/orange). **B:** Chromaticity diagram (**a**) and specific colors (**b**) generated by SiO_2 nanoparticles containing different ratios between naphthalimide and tetrazine. Note the SiO_2 nanoparticles denoted NPC, which contained approximately 2:1 ratio between naphtalimide and tetrazine, generating almost pure white color. Reprinted with permission from Malinge et al., *Angew. Chem. Int. Ed. Eng.* **51** (2012), 8534–8537, © 2012 John Wiley & Sons.

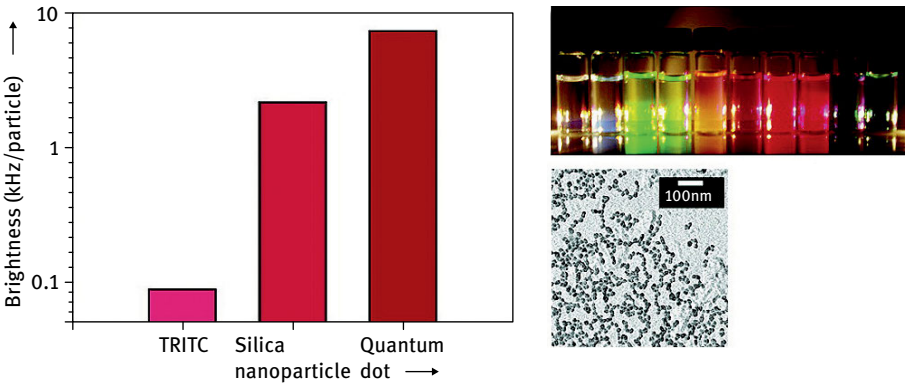

Fig. 4.33: Bright colors of core-shell silicon oxide nanoparticles containing different fluorescent dyes. **Left:** comparison of the brightness of dye-encapsulated silicon oxide nanoparticles (middle column) to the bare dye (left column) or conventional quantum dots (right column). **Right:** Encapsulation of different dyes in the core shell silicon oxide nanoparticles produces different colors; an electron microscopy image of the nanoparticles (bottom). Reprinted with permission from Ow et al., *Nano Lett.* **5** (2005), 113–117, © 2005 American Chemical Society.

been used in diverse applications as catalysts, sensors, filters, and more. Similar to other chemical systems, the advent of nanoscale science and technology has led to the discovery of unique properties and applications associated with rare earth oxide nanoparticles. In particular, significant activity in this field has focused on biological and biomedical applications, discussed below.

Cerium oxide (CeO_2) NPs have garnered significant interest in light of their therapeutic potential and diverse biological applications. Most synthetic methods of producing CeO_2 NPs rely on the prevalence of the Ce^{4+} oxidation state of cerium, using precursors containing this ion. An elegant micro-emulsion CeO_2 NP synthesis method demonstrated by J. J. Hickman and colleagues at the University of Central Florida is illustrated in Figure 4.34. The Ce^{4+} precursors were injected into the solution of a nonpolar solvent and surfactants, yielding micelles stabilized by the surfactant molecules and enclosing aqueous solutions containing the precursors. The micelles then served as "nanoreactors" for slow assembly of the crystalline CeO_2 NPs.

CeO_2 NPs display unique biocatalytic properties which correlate with the ready conversion between the Ce^{4+} and Ce^{3+} oxidation states. Cerium predominantly exists as Ce^{4+}, and accordingly most crystal lattice sites within CeO_2 NPs are occupied by this ion. However, a certain portion of cerium ions in the crystal adopt the Ce^{3+} oxidation state. As a consequence, "lattice defects" (also referred to as oxygen "vacancies") occur within crystalline CeO_2 NPs, since fewer oxygen molecules are required in the crystal lattice for electrostatic balance (as oxygen exhibits the negative charge compensating for the positive cerium ions; see Fig. 4.35).

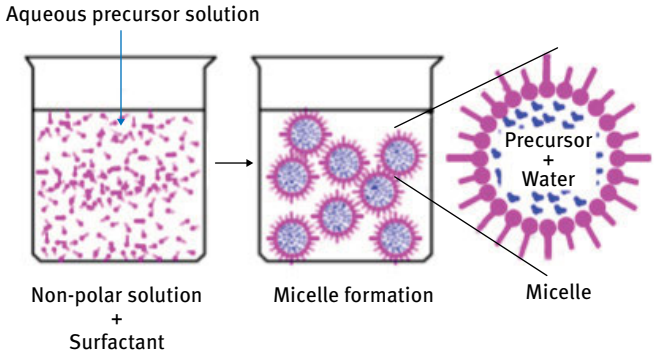

Fig. 4.34: Cerium oxide nanoparticles produced via a micro-emulsion methodology. Micelles containing aqueous solution and the CeO_2 nanoparticle precursors act as "nanoreactors" for nanoparticle formation. Reprinted from Das M. et al., Auto-catalytic ceria nanoparticles offer neuroprotection to adult rat spinal cord neurons, *Biopolymers* **28** (2007), 1918–1925, with permission from Elsevier.

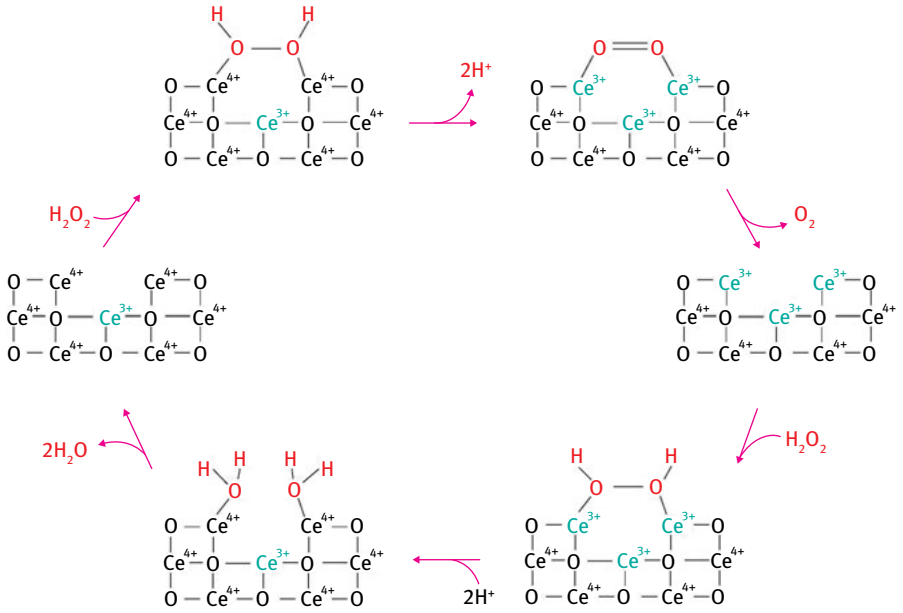

Fig. 4.35: Catalysis of hydrogen peroxide degradation by cerium oxide nanoparticles. A proposed cycle of oxidative disintegration of H_2O_2 through docking of the molecules at oxygen "vacancies" and subsequent electron transfer to Ce^{4+} at the CeO_2 nanoparticle framework. Ce^{4+} ions in the crystal lattice are indicated in black and Ce^{3+} ions are shown in green. Figure inspired by Celardo et al., *Nanoscale* **3** (2011), 1411–1420.

The oxygen vacancies and Ce^{3+}/Ce^{4+} redox transformations constitute the key factor underlying the catalytic properties of CeO_2 NPs. In particular, these vacancies, prevalent at the NP surface, promote adsorption (or "scavenging") of cell-damaging oxygen radicals (generally referred to as reactive oxygen species, ROS) and oxidizing species (e.g. molecules which tend to inflict physiological damage through electron extraction), which are then catalytically decomposed. Figure 4.35 depicts a proposed catalytic mechanism for removal of H_2O_2 by CeO_2 NPs. H_2O_2 (hydrogen peroxide) is a potent oxidant believed to contribute to oxidative stress pathways (for example neuronal cell destruction occurring in ischemic stroke). In essence, the oxygen vacancies within the CeO_2 NP framework serve as binding sites for the hydrogen peroxide molecules (or other oxygen-containing radical species). As shown in Figure 4.35, subsequent oxidation/reduction steps eliminate the bound H_2O_2 via generation of protons and water molecules released to the solution. It should be emphasized that the cycle depicted in Figure 4.35 is *autocatalytic* – the CeO_2 NPs are continuously regenerated by water and oxygen release. Furthermore, the redox process catalyzed by the CeO_2 NPs is chemically similar to enzymatic reactions responsible for H_2O_2 degradation, underscoring the "biomimetic" features and therapeutic potential of CeO_2 NPs.

While the anti-oxidant and radical scavenging activities of CeO_2 NPs as depicted in Figure 4.35 have been intensively studied in various model systems, the "redox cycling" mechanism (and other putative anti-oxidative processes involving the CeO_2 NPs) has not been unequivocally proven in vivo (e.g. in actual situations occurring in the human body). Furthermore, the toxicity of CeO_2 NPs themselves needs to be assessed, as the material could induce electron transfer and harmful side reactions with other bio-molecules. Moreover, the anti-oxidant properties of CeO_2 NPs might actually aid survival of cell species proliferating in oxidative stress conditions, for example cancer cells. Overall, however, CeO_2 NPs are considered promising candidates for new therapeutic treatments of diverse diseases and pathological conditions such as ischemic stroke, and their introduction to mainstream biomedicine is steadily progressing.

The "scavenging" mechanisms associated with CeO_2 NPs have been exploited not only as potential therapeutic platforms, but also for applications such as biosensing. Figure 4.36, for example, illustrates a colorimetric paper-based glucose sensor based on the color changes induced on H_2O_2 adsorption onto CeO_2 NPs. The sensing concept, introduced by S. Anreescu and colleagues at Clarkston University, US, utilized CeO_2 NPs coupled to the enzyme *glucose oxidase* immobilized on a paper-supported matrix (Fig. 4.36). Oxidation of glucose (the target analyte) by the embedded glucose-oxidase yielded hydrogen peroxide (H_2O_2), which in turn was adsorbed onto the CeO_2 NPs. Importantly, CeO_2 NPs containing surface-adsorbed H_2O_2 exhibit a darker orange-brown color (in comparison with the yellowish appearance of the as-synthesized CeO_2 NPs), making visual detection of glucose by the CeO_2 NPs/glucose-oxidase/paper assay possible.

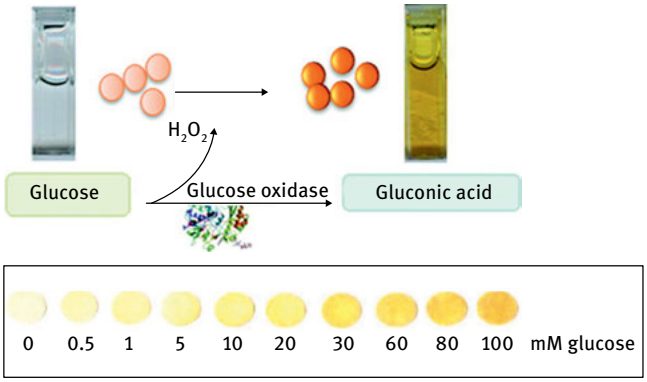

Fig. 4.36: Glucose sensing by cerium oxide nanoparticles. The sensor assembly comprises of CeO_2 nanoparticles and the enzyme glucose oxidase, both immobilized within a paper matrix. The experimental scheme (top) is based on oxidation of glucose by the glucose oxidase enzyme, producing H_2O_2 which gets adsorbed onto the CeO_2 nanoparticles. Following adsorption of H_2O_2, the CeO_2 nanoparticles undergo a visible yellow-brown color change. The scanned image shows the visible color transitions of the CeO_2 nanoparticle paper sensor in the presence of different glucose concentrations. Reprinted with permission from Ornatska et al., *Anal. Chem.* **83** (2011), 4273–4280, © 2011 The American Chemical Society.

Gadolinium oxide (Gd_2O_3) NPs have been the most effective *contrast agents* in magnetic resonance imaging (MRI), and as such play an extremely important role in biomedicine. Gadolinium is the element with the largest number of unpaired electrons in the outer shell (seven electrons), allowing efficient magnetic coupling to protons in close proximity and consequent faster relaxation of the proton magnetization. Accordingly, contrast agents containing Gd^{3+} (generally referred to as "positive-T_1" contrast agents) enhance MRI images by increasing the rate of magnetic relaxation of adjacent water protons in tissues (and thus enabling application of faster magnetic pulses and consequently higher signals). While Gd^{3+} ions by themselves are toxic, chelated (i.e. complex-forming) gadolinium is considered safe, and is the most routinely and widely used MRI contrast agent. Gd_2O_3 NPs, in this context, also offer distinct advantages as effective and medically-safe contrast agents.

"Ultra-small" Gd_2O_3 NPs (US-Gd_2O_3; in the range of 2–3 nm) have attracted particular interest as MRI contrast agents. These NPs contain relatively large numbers of gadolinium ions within the very small volume of the particle, thus exhibiting, in principle, good contrasting capacity. Figure 4.37 highlights the fact that Gd^{3+} ions are abundant on the surface of US-Gd_2O_3 NPs, thus affecting the magnetic relaxation of protons in neighboring water molecules to a greater extent than conventional water-soluble Gd^{3+} complexes. Furthermore, the size of US-Gd_2O_3 NPs (significantly larger than chelated Gd^{3+} complexes) and their stability in physiological environments leads to slower removal from the targeted tissues and longer circulation times within the bloodstream, thereby prolonging imaging times and efficiencies.

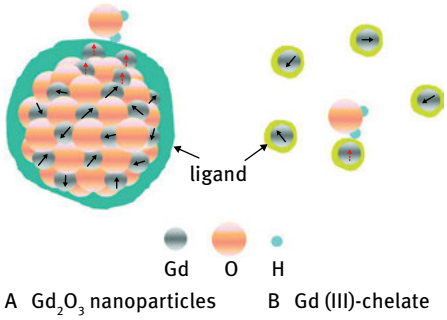

Fig. 4.37: Gadolinium oxide nanoparticles as contrast agents in magnetic resonance imaging (MRI). The large number of Gd^{3+} ions at the surface of Gd_2O_3 nanoparticles induce more effective relaxation of protons within adjacent water molecules as compared to conventional Gd^{3+}-containing complexes, which exhibit smaller surface area and lower interface with water molecules. Reprinted with permission from Park et al., *ACS Nano* **3** (2009), 3663–3669, © 2009 The American Chemical Society.

As with other nanoparticle species, optimizing biocompatibility and endowing targeting capabilities are considered critical issues to make Gd_2O_3 NPs an effective imaging tool. Research in this field generally focuses on creating "hybrid" Gd_2O_3 NPs which comprise of additional (usually bio-active) components. A common approach has been to coat the Gd_2O_3 NP core with layers containing biological recognition elements, and/or additional reporting molecules such as fluorescence dyes. Figure 4.38, for example, shows the imaging capabilities of Gd_2O_3 NPs coated with a polysiloxane shell (a silicon-oxide matrix which further hosted fluorescent dyes). The nanoparticles, synthesized by S. Roux and colleagues at Universite Claude Bernard, Lyon, France, provided dual imaging platforms – both fluorescence and MRI enhancement. In particular, the MRI data in Figure 4.38 show that image enhancement was inversely correlated to NP diameter; consistent with the contribution of the NP/water interface to proton magnetic relaxation and signal enhancement (i.e. larger nanoparticles provide less overall surface area). The experiments further indicate that the silicon-oxide shell did not adversely affect the image enhancement capabilities of the NPs.

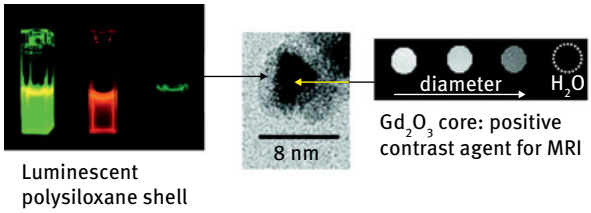

Fig. 4.38: Gadolinium oxide nanoparticles coated with luminescent shells. The core-shell nanoparticles comprise of Gd_2O_3 cores and polysiloxane shells which further embed a fluorescent dye. Enhancement of magnetic resonance imaging (MRI) signal by the core-shell nanoparticles is shown in the right photograph. Greater enhancement is recorded in solutions of smaller-diameters particles, consistent with the significance of surface-to-volume ratio in affecting the magnetic relaxation of water protons and corresponding MRI signal enhancement. Reprinted with permission from Bridot et al., *JACS* **129** (2007), 5076–5084, © 2007 The American Chemical Society.

4.6 Other metal oxide nanoparticles

Other metal oxide NP systems have been developed. *Tin dioxide* (SnO_2) is a wide bandgap semiconductor material used in varied applications, including solar cells, photocatalysis, gas sensing, and others. Similar to the ZnO and TiO_2 NPs, discussed above, SnO_2 nanoparticles may have useful roles in photocatalysis and sensing applications. Indeed, SnO_2 NPs are particularly advantageous for such applications since they are chemically and physically stable over time, and exhibit high surface area – favorable for large-scale adsorption of substrates for catalytic degradation or target analytes in sensing applications (particularly gas sensing).

The operation principle of SnO_2 NP-based gas sensors is modulation of the electrical resistance of the sensor films induced by surface adsorption of gas molecules. In this context, modifying the surface morphology and surface areas of SnO_2 NPs has been found to intimately affect the performance of such sensors. Figure 4.39 shows electron microscopy images of SnO_2 NPs with octahedral morphology exhibiting higher gas detection sensitivity, presumably due to greater adsorption of gas molecules onto the flat crystalline facets of the particles. Furthermore, Z. Xie and colleagues at Xiamen University, China, who synthesized the NPs, discovered that the sensor response was lower in cases where the NPs had an *elongated* morphology (Fig. 4.39B); this observation was ascribed to the distinct atomic organization of the exposed facets within each NP configuration. Specifically, the researchers hypothesized that the elongted NP structure has a lower abundance of tin ions with "dangling bonds" – i.e. ions which are not bonded to oxygen – available to anchor gas molecules.

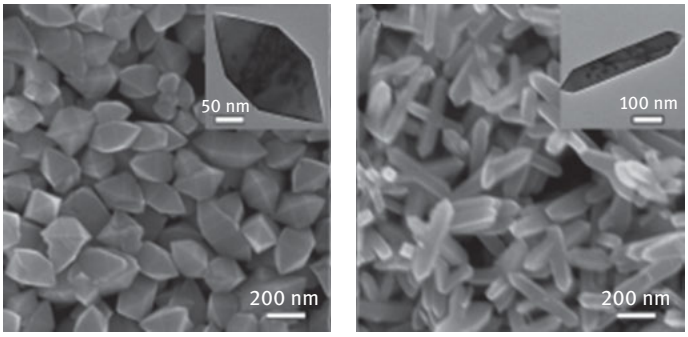

Fig. 4.39: Octahedral tin oxide nanoparticles. The elongated SnO_2 nanoparticles adsorb smaller numbers of gas molecules, presumably due to lower abundance of nonbonded Sn^{4+} available for binding. Reprinted with permission from Han et al., *Angew. Chem Int. Ed.* **48** (2009), 9180–9183, © 2009 John Wiley & Sons.

Other types of SnO_2 NP-based gas sensors have been reported. Figure 4.40 illustrates a gas sensor based on a porous matrix comprising of SnO_2 NPs coupled to glucose molecules. The glucose residues functioned here as stabilizers of the porous framework, essential for facilitating adsorption of the target analytes. This composite SnO_2 NP/glucose framework, reported by S. V. Manorama and colleagues at the Indian Institute of Chemical Technology, Hyderabad, displayed superior photocatalytic properties – attributed to the high surface area of the NPs available for adsorption, interspersed within the porous and transparent matrix.

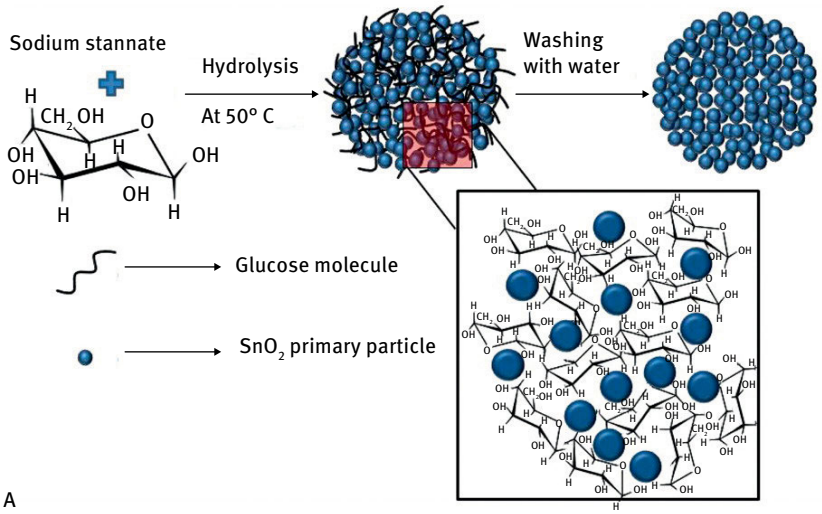

A

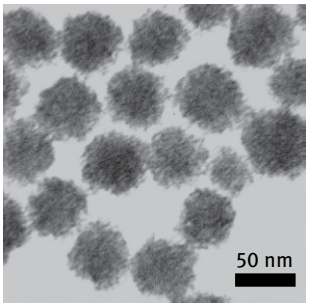

B

Fig. 4.40: Tin oxide nanoparticles/glucose porous assembly for gas sensing. Coupling of the nanoparticles and glucose molecules yields a porous framework promoting adsorption of gas molecules. The electron microscopy image shows the sponge-like morphology of the nanoparticles. Reprinted with permission from Manjula et al., *ACS Appl. Mater. Interfaces* **4** (2012), 6252–6260, © 2012 American Chemical Society.

SnO_2 nanowires (NWs) have also been employed as platforms for gas sensing. Interestingly, several studies have reported significant enhancement of the sensing capabilities of SnO_2 NWs which were doped with *metal* NPs. Figure 4.41, for example, illustrates a gas sensor setup constructed by A. Kolmakov and colleagues at the University of California, Santa Barbara, in which a SnO_2 NW placed between the source and drain was doped with palladium (Pd) nanocrystals. The doped SnO_2 NWs were found to be much more sensitive as sensors for oxygen gas compared to bare SnO_2 nanowires. This phenomenon was ascribed to the catalytic properties of the Pd nanoparticles (see Chap. 3), resulting in rapid disintegration of surface-adsorbed O_2 molecules and subsequent diffusion of the resultant atom products which alter the resistivity of the NWs.

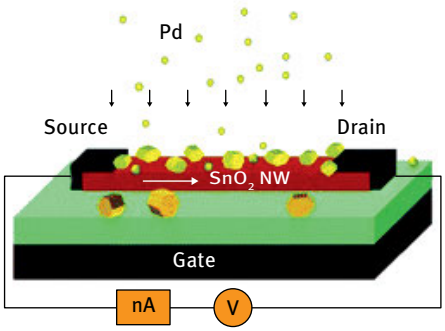

Fig. 4.41: Metal-doped tin oxide nanowire gas sensor. Doping of the SnO_2 nanowire by palladium nanocrystals is carried out following placement of the nanowire in the transistor device. The doped nanowire displayed higher sensitivity as a gas (oxygen) sensor. Reprinted with permission from Kolmakov et al., *Nano Lett.* **5** (2005), 667–673, © 2005 American Chemical Society.

Indium tin oxide (ITO) NPs have garnered significant interest due to the prominence of ITO in numerous electro-optical devices and applications. ITO is at present the main material in transparent conductive electrodes (TCEs) and transparent conductive films, essential components in solar cells, electro-optical devices, and more. ITO usage in such devices is due to the wide bandgap of In_2O_3, a semiconductor, which minimizes light absorbance in the visible spectral region (thus making ITO transparent). In addition, the "crystal defects" – usually oxygen vacancies – within the In_2O_3 lattice and distortions of crystal organization induced by doping with tin ions (Sn^{4+}) promote electron transport and contribute to the enhanced electrical conductivity of ITO.

Research focused on ITO nanoparticles partly stems from practical reasons. ITO NPs can easily be synthesized in solution via a thermally-induced reaction between indium and tin precursors, yielding particles with tunable size distributions. ITO NPs can then be deposited on varied substrates, forming uniform films. Indeed, the availability of simple, inexpensive, and scalable solution-phase NP deposition techniques such as *spin casting* (deposition of a NP-containing solution on a spinning surface, followed by evaporation of the solvent) could provide a powerful alternative for existing ITO film fabrication methods which are technically-demanding, expensive, and often environmentally hazardous. Figure 4.42 illuminates the fabrication of a highly transparent conductive film comprising ITO NPs using a polymer substance as a tem-

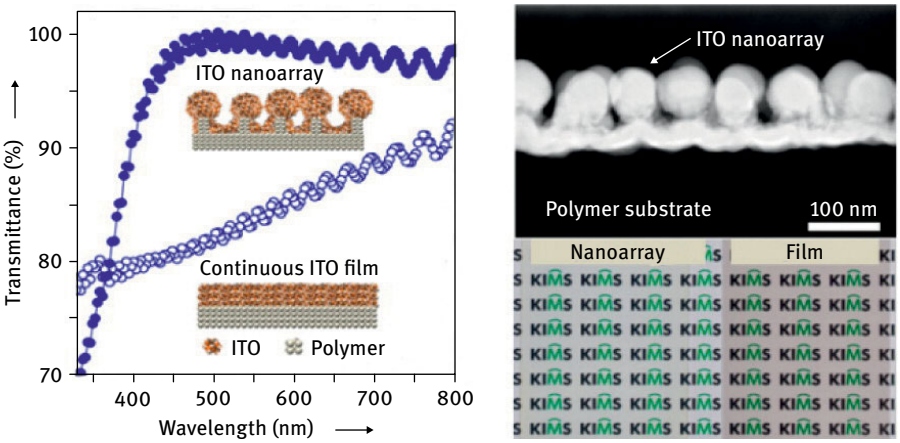

Fig. 4.42: Transparent conductive films from indium thin oxide (ITO) nanoparticles. The ITO nanoparticles were deposited on a patterned polymer substrate from the vapor phase creating an ITO nanoarray (microscopy image on the right). The transmittance graph on the left demonstrates that the nanoparticle film featured significantly higher optical transparency compared to conventional continuous ITO films. Reprinted with permission from Yun et al., *ACS Appl. Mater. Interfaces* **5** (2013), 164–172, © 2013 American Chemical Society.

plate. The films were prepared by J. Yun and colleagues at The Korea Institute of Materials Sciences by vapor deposition (sputtering) of the ITO NPs on a polymer substrate which was sculpted to include protruding "pillars". The patterned ITO NP films exhibited excellent conductivity and transparency ascribed to the "openings" between the deposited NPs.

Tunable surface plasmon resonance (SPR) has been another interesting phenomenon observed in ITO NPs. Described in more detail in Chapter 3, SPR results from interaction between light and partly-free electrons present at NP surfaces, producing in many instances visible colors of NP suspensions (depending on the wavelength of the plasmon resonance). While SPR has mostly been recorded in metallic NPs (primarily Au NPs), it is also generated in metal oxide NPs such as ITO NPs, attributed in such semiconductor NPs to free electrons excited by light to the conduction band. Interestingly, the percentage of tin in ITO NP compositions was shown to be the likely main parameter for tuning SPR in ITO NPs, essentially determining the color of the NP suspensions. Figure 4.43 depicts suspensions of ITO NPs created by S. Sun and colleagues at Brown University, displaying different colors which were dependent upon the mole percentage of tin in the particles.

Transition metal oxide NPs are among the most diverse NP families in terms of structure, chemical and physical properties, and macro-scale organization. This variety emanates from the diversity of transition metal elements themselves – their oxidation states, electronic structures, and crystal organizations. *Manganese oxide NPs* appear in diverse morphologies, in large part because of the several oxidation

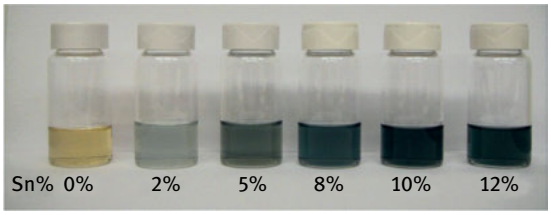

Fig. 4.43: Color of indium tin oxide (ITO) nanoparticle suspensions depends on percentage of tin in the nanoparticles. The solution color reflects the surface plasmon resonance (SPR) associated with the particles. Reprinted with permission from Lee et al., *JACS* **134** (2012), 13410–13414, © 2012 American Chemical Society.

states of manganese available. Figure 4.44 depicts MnO_2 nanowires self-assembled into a dense "free-standing" (i.e. non solid-supported) membrane. These extremely long nanowires, synthesized by L. Yu and colleagues at Guangdong University of Technology, China, were homogeneous, could be dissolved in water, and formed intertwined stable membranes after drying in a vacuum. Notably, the MnO_2 nanowire membrane could be further functionalized. For example, incorporation of *magnetic nanoparticles* within the nanowire matrix (Fig. 4.44B), gave rise to formation of a functional "magnetic membrane".

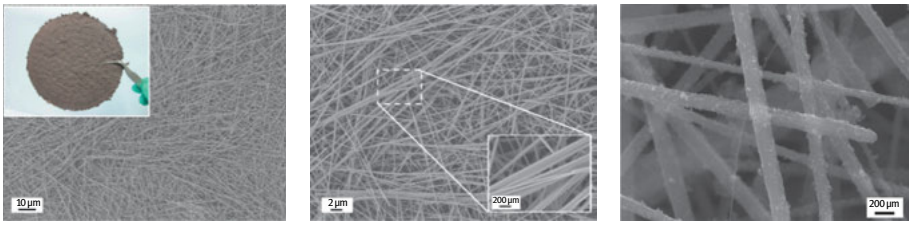

A B

Fig. 4.44: Manganese oxide nanowires. **A:** Dense free-standing mesh of MnO_2 nanowires; **B:** MnO_2 nanowires doped with magnetic nanoparticles (shown as white specks). The doped nanowire matrix becomes magnetic. Reprinted with permission from Lee et al., *ACS Appl. Mater. Interfaces* **5** (2013), 7458–7464, © 2013 American Chemical Society.

While MnO_2 is the most abundant, naturally-occurring manganese-containing mineral, the Mn^{2+} oxidation state is actually more common in manganese compounds. MnO NPs, in particular, have displayed intriguing properties and structures. Figure 4.45A shows electron microscopy images of multipod MnO NPs, synthesized by D. Zitoun and colleagues at Universite Montpellier II, France. These unconventional NP structures, observed also in binary semiconductor NPs (see Chap. 2), are believed to occur by a two-step crystallization process. First, the multipod core is formed around nucleating seeds in solution. The subsequent anisotropic growth of the "arms" is

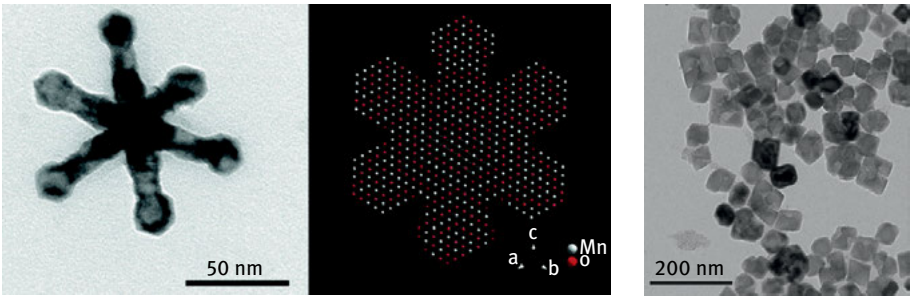

Fig. 4.45: Multipod manganese oxide nanoparticles. **A:** Electron microscopy image of MnO hexapod (left) and a schematic depiction of manganese and oxygen atoms in the crystal lattice (right); **B:** Cubic MnO nanoparticles produced following a short reagent incubation time. This result supports the mechanism in which the multipod synthesis starts with crystallization of the core, followed by growth of the arms. Reprinted with permission from Zitoun et al., *JACS* **27** (2005), 15034–15035, © 2005 American Chemical Society.

governed by differences in reactivity of the crystal facets of the core. Corroborating this hypothesis was the observation that polyhedral "cores" without protruding arms were produced following shorter synthesis duration.

Copper (cupric) oxide (CuO) NPs constitute a class of semiconductor NPs distinctive as low bandgap materials (in contrast to most metal oxides which exhibit high energy bandgaps). The *p-type* semiconductor CuO NPs exhibit useful properties, such as sensing when coupled to *n-type* semiconductor oxides (e.g. ZnO or SnO_2), related to the formation of "p-n junctions" in such constructs. The electric field which develops in p-n junctions – e.g. the interface between the p-type semiconductor contributing holes and the electron-providing n-type semiconductor – usually translates into narrower conduction bands of the semiconductor sensor leading to enhanced sensitivity following adsorption of (gas) molecules. An example of such a sensor device is shown in Figure 4.46. The sensor, developed by J. Chen and colleagues at the University of

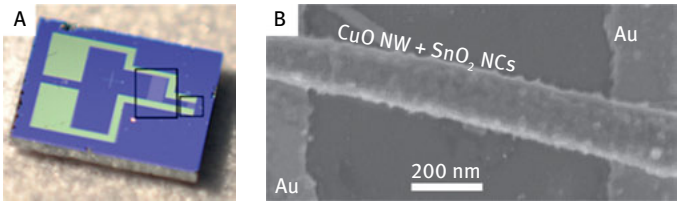

Fig. 4.46: Cupric oxide nanowire doped with tin oxide nanocrystals used in a sensor device. Doping of the p-type CuO nanowire with n-type SnO_2 nanoparticles increases the sensitivity of the sensor due to formation of p-n junctions. Reprinted with permission from Lee et al., *ACS Appl. Mater. Interfaces* **4** (2012), 4192–4199, © 2012 American Chemical Society.

Wisconsin, comprised of a single CuO nanowire doped with SnO_2 NPs (which form p-n junctions with the CuO NW). Adsorption of gas molecules onto the NW surface gave rise to greater modulation of the resistance of the NW device in comparison with un-doped CuO nanowires.

Vanadium oxide NPs have been used in various applications, from catalysts to antibacterial agents. *Vanadium pentoxide (V_2O_5) nanowires*, in particular, have been touted as promising "anti-fouling" agents, on account of their capacity to prevent formation of bacterial biofilms – the resilient impenetrable matrix formed by many bacterial species on surfaces. This inhibitory action has been ascribed to interference with bacterial communication pathways important in biofilm formation. As an example, W. Tremel and colleagues at the Johannes Gutenberg-University, Germany, demonstrated that V_2O_5 nanowires could act as anti-fouling agents (Fig. 4.47).

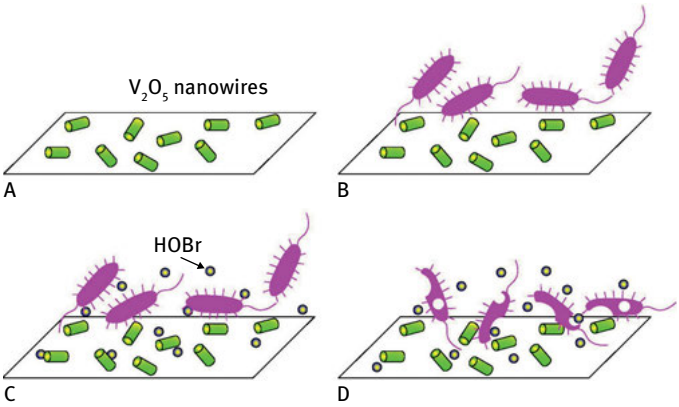

Fig. 4.47: Vanadium oxide nanowires acting as anti-bacterial agents. **A:** V_2O_5 nanowires are deposited on a surface. **B:** Bacteria near the surface aim to establish colonies. **C:** In the presence of Br^- and H_2O_2, the V_2O_5 nanowires catalyze production of HOBr (yellow spheres), an antibacterial agent. **D:** The bacterial cells are destroyed. Figure inspired by Natalio et al., *Nature Nanotech.* **7** (2012), 530–535.

Specifically, the V_2O_5 NWs catalyze the oxidation/reduction reaction between hydrogen peroxide (H_2O_2) and Br^- ions according to the equation

$$H_2O_2 + Br^- + H^+ \rightarrow HOBr + H_2O.$$

HOBr (hypobromous acid) is known as an effective anti-bacterial compound, as it adversely affects intercellular bacterial signaling processes which play crucial roles in generating bacterial biofilms (also known as "quorum sensing" processes). Indeed, researchers demonstrated that surface deposition of V_2O_5 nanowires and co-addition of bromide salt resulted in pronounced inhibition of bacterial adhesion and blocking of biofilm formation (i.e. the nanowires acted as anti-fouling agents).